REPORT DOCUMENTATION PAGE

Form Approved
OMB No. 0704-0188

1. AGENCY USE ONLY (Leave blank)	2. REPORT DATE 31 May 96	3. REPORT TYPE AND DATES COVERED Final 15 Jan 93 to 14 Apr 96

4. TITLE AND SUBTITLE
Quantum Optical Studies of Semiconductors

5. FUNDING NUMBERS
61102F
2301/AS

6. AUTHOR(S)
Duncan G. Steel

AFOSR-TR-96

$O 333$

7. PERFORMING ORGANIZATION NAME(S) AND ADDRESS(ES)
University of Michigan
Dept of Electrical Engineering and Computer Science
Ann Arbor, MI 48109

9. SPONSORING/MONITORING AGENCY NAME(S) AND ADDRESS(ES)
Air Force Office of Scientific Research - NE
Building 410
Bolling AFB, DC 20332

10. SPONSORING/MONITORING AGENCY REPORT NUMBER
F49620-93-1-0115

11. SUPPLEMENTARY NOTES

19960627 057

12a. DISTRIBUTION/AVAILABILITY STATEMENT

Approved for public release; distribution unlimited.

12b. DISTRIBUTION CODE

13. ABSTRACT (Maximum 200 words)

There have been two primary objectives during the current program: 1) The development and application of nonlinear laser spectroscopy to the study of excitation dynamics near the band edge of semiconductor heterostructures; 2) The understanding of pump noise suppression for production of number squeezed states of the laser field from quantum-well lasers for application to low noise experiments.

Our progress in the study of GaAs structures has relied on an approach employing both high-resolution frequency-domain and picosecond/femtosecond coherent nonlinear spectroscopy. We have obtained new understanding of the dynamics and energy level structure associated with excitons particularly as these properties are affected by disorder and magnetic fields. Our work in bulk GaAs shows that the nonlinear response at moderate densities is due to dynamic exciton-exciton interactions which lead to a nonlinear response proportional to the effective exciton-exciton collision cross-section. These experiments have been paralleled with new understanding regarding the role of quantum coherences in the optical properties of these systems.

Our studies of noise reduction below the standard quantum limit have resulted in our achieving 95% of the theoretically predicted limit for number-state squeezing in a quantum-well laser (4.5 dB below shot-noise, 5.9 dB corrected to the facet). We have also made a preliminary demonstration of an application to semiconductor spectroscopy in the study of the Urbach tail in a GaAs multiple quantum-well structure.

DTIC QUALITY INSPECTED 1

14. SUBJECT TERMS
Semiconductors, Laser spectroscopy, Quantum optics

15. NUMBER OF PAGES
37

16. PRICE CODE

17. SECURITY CLASSIFICATION OF REPORT	18. SECURITY CLASSIFICATION OF THIS PAGE	19. SECURITY CLASSIFICATION OF ABSTRACT	20. LIMITATION OF ABSTRACT
UNCLASSIFIED	UNCLASSIFIED	UNCLASSIFIED	UL

DISCLAIMER NOTICE
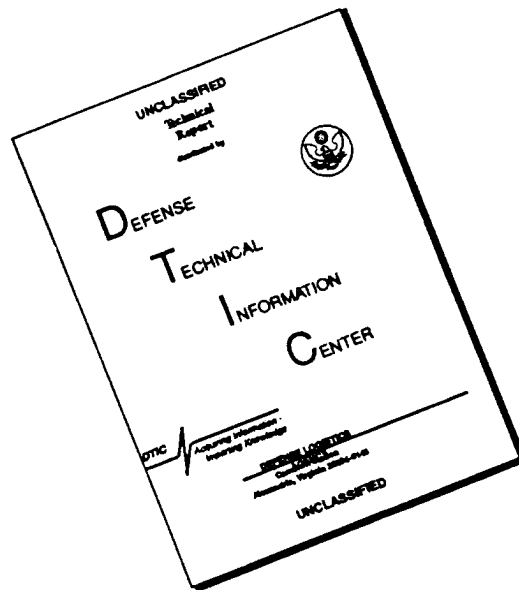
THIS DOCUMENT IS BEST QUALITY AVAILABLE. THE COPY FURNISHED TO DTIC CONTAINED A SIGNIFICANT NUMBER OF PAGES WHICH DO NOT REPRODUCE LEGIBLY.

FINAL REPORT
to
THE AIR FORCE OFFICE OF SCIENTIFIC RESEARCH

Program Title: Quantum Optical Studies of Semiconductors

Principal Investigator: Duncan G. Steel
Department of Electrical Engineering and Computer Science
Department of Physics
Harrison M. Randall Laboratory of Physics
The University of Michigan
Ann Arbor, MI 48109
Phone: 313-764-4469
Email: dst@umich.edu

I. A. RESEARCH OBJECTIVES:

The objective of this program has been to conduct research studies into the quantum optical aspects of semiconductor systems. The research emphasizes experimental and theoretical work in two related areas of the optical physics of semiconductors. In the first part of the program, we investigated nonlinear optical phenomena in semiconductors where we are particularly interested in characterizing, at the fundamental physics level, the origin of the nonlinear optical response as well as physics associated with important relaxation processes. In the second part of the program, we explored development of experiments in the quantum optics of semiconductor lasers based primarily on the study and application of amplitude squeezed light.

I.B. STATUS OF EFFORT:

Experimental and theoretical work is continuing based on funding by AFOSR of a renewal proposal entitled "Quantum Optical Studies of Semiconductors" along with an associated AASERT Program. Research focuses on using the understanding the developed on this and earlier programs to initiate new work in the area of studies of the full optical response of disordered semiconductor heterostructures and semiconductor nanostructures.

I.C. SUMMARY OF RECENT RESULTS:

In the first area associated with our studies of nonlinear optical physics in semiconductors, our research has underscored the major and unexpected role of inherent growth- and process-induced disorder in determining the nonlinear response. Hence we found that complimentary experiments in high-quality bulk GaAs have been critical to facilitate our understanding of the *intrinsic* response and provide crucial insight into the effects of confinement and disorder in heterostructures.

Our progress in the study of GaAs structures has relied on an approach employing both high-resolution (cw) frequency-domain and (transient) picosecond/femtosecond coherent and incoherent nonlinear spectroscopic techniques such as hole burning, stimulated photon echoes, time-resolved free polarization decay, and spectrally-resolved differential transmission (DT) measurements. We have obtained new understanding of the dynamics and energy level structure associated with excitons in GaAs/AlGaAs quantum-wells, particularly as these properties are affected by disorder and magnetic fields. More recently, however, our work in bulk GaAs shows for the first time that the nonlinear response in this system at moderate densities is due to dynamic exciton-exciton interactions which lead to a nonlinear response proportional to the effective exciton-exciton collision cross-section.

In the second area, our studies of noise reduction below the standard quantum limit (SQL) have resulted in our achieving 95% of the theoretically predicted limit for number-state squeezing in a quantum-well laser(4.5 dB below shot-noise, 5.9 dB corrected to the facet) based on the independently determined quantum efficiency. We have also demonstrated that these lasers can be amplitude-modulated without loss of squeezing, and we have made a preliminary demonstration of an application to semiconductor spectroscopy in the study of the Urbach tail in a GaAs multiple quantum-well structure.

Some of the more important results are summarized below (discussed in more detail in Section II):

Studies of exciton-exciton interactions:

In collaboration with the theoretical group directed by Stephan Koch (previously at the University of Arizona and now at the University of Marburg), we have performed a

series of experiments on the heavy hole (*hh*1) exciton in (strained) GaAs to demonstrate that the nonlinear optical response is due to exciton-exciton scattering which leads to dephasing of the exciton coherence, a behavior identified as excitation-induced dephasing (EID) and similar to resonant collisional broadening in atomic vapors. We have shown that the nonlinear susceptibility is proportional to the exciton-exciton scattering cross-section, and this observation led to the inclusion of scattering terms previously ignored in the semiconductor Bloch equations. These results are critical in explaining the dependence of the nonlinear response on the polarization of the incident beams, behavior which could not be reconciled with the original semiconductor Bloch equations (SBE).

The effects of excitation-induced dephasing were also included in the ordinary optical Bloch equations (OBE). The solution of these modified OBE then provided a simple physical picture for the interpretation of experimental behavior and comparison with other nonlinear optical effects in dense systems, such as local fields. The equations also permitted an analytic solution which gave excellent agreement with experiments in bulk GaAs.

The more detailed SBE were applied to the complex quantum-well system for insight into the polarization dependence of the signal measured in our experiments.

High-resolution FWM polarization-sensitive spectroscopy was performed in bulk GaAs and showed clear evidence of a red-shifted resonance at both the *lh*1 exciton and the *hh*1 exciton. Based on numerous measurements, this resonance is believed to arise from the biexciton. The *lh-lh* biexciton binding energy obtained is ~0.2 meV.

Coherent transient spectroscopy studies of the biexciton resonance based on interferometric studies of the FWM response showed evidence of the coherent oscillation of the quantum coherence at 1.3 fsec (770 THz) corresponding to the coherent two-photon excitation of the biexciton.

Using spectrally nondegenerate transient FWM, we demonstrated the existence of the heavy-hole-light-hole quantum coherence and the unexpectedly fast dephasing time showing uncorrelated scattering between the two bands.

Nonlinear magneto-optical properties of GaAs:

We have probed the nonlinear magneto-optical response of Wannier excitons in bulk GaAs at 4 K. The results show a large enhancement in the nonlinear optical response related to a field-induced decrease in exciton mobility due to magnetic freeze-out.

High-resolution cw nonlinear spectroscopy was used to measure the relative strength of inter-Landau level coupling and showed that the nonlinearity is dominated by Coulomb effects.

Number-state squeezing:

Based on the work of Yamamoto and in collaboration with Spectra Diode Laboratories, we have made the first demonstration of number-state squeezing in quantum-well lasers. Our most recent studies show 4.5 dB (5.9 dB corrected) of squeezing below the SQL.

Wavelength tunable number-state squeezed emission was demonstrated using either an external cavity or injection locking. This work demonstrated that the dominant noise preventing the theoretical maximum in squeezing arises from below-threshold side modes.

Of importance to the eventual application of these lasers is our demonstration that these lasers can be amplitude-modulated without loss of squeezing.

Measurements of the polarization properties of the noise show the presence of strong correlations which must be accounted for in order to achieve maximum squeezing. The results show that at least a part of the observed correlations are intrinsic to the laser and may be quantum in origin.

Using these lasers, we performed the first demonstration of spectroscopy below the standard quantum limit using amplitude squeezed states. Measurements were performed using coherent nonlinear spectroscopy of excitons and the Urbach tail in GaAs.

In Section II, we describe in more detail the essential experimental progress during the past three years.

II.A.   RESEARCH SUMMARY

II.A.1. STUDIES OF EXCITON-EXCITON INTERACTIONS

At low excitation densities and temperatures the nonlinear optical response near the band edge in direct-gap semiconductors is dominated by excitonic effects, including effects due to Pauli exclusion (phase space filling and exchange) and Coulomb interactions (e.g., screening). The relative importance of these many-body properties remains under intense study using ultrafast four wave mixing (FWM) techniques. The interpretation of most FWM results has been based on purely coherent effects and many-body interactions such as the static exchange interaction.

In materials like GaAs quantum-wells or strained bulk GaAs, additional information can be extracted from FWM data, if one takes into account the polarization dependence of the two-fold degenerate excitons, such as the heavy hole excitons, which include the valence bands with (pseudo) angular momentum states $m_j=\pm 3/2$. The optical selection rules for these systems have been thoroughly investigated. FWM experiments studying the optical selection rules have focused mainly on spin-flip processes. By the end of the previous three-year program, however, our group and others recognized that the dependence of the nonlinear signal on the polarization (linear or circular) of the input beams was very complex and could not be described by the current models of the excitonic response. More precisely, the well-established semiconductor Bloch equations could not be immediately extended to a *vectorial* form to account for the pronounced effects that were observed as a function of incident polarization.

These discrepancies were observed very clearly in our laboratory by studying the time-resolved emission in a transient FWM experiment. Specifically, as we noted in an earlier paper on this program, in high-quality 10-period multiple-quantum-wells (<1 meV absorption linewidth and negligible luminescence Stokes shift) the co-linearly polarized and cross-linearly polarized responses were distinctly different in their temporal features. The co-polarized response (the first two incident fields, E_1 and E_2, were linearly co-polarized $E_1 \parallel E_2$ and designated $FWM_\parallel$) observed at low excitation density (<10^9 excitons/cm^2) was a stimulated photon echo with a slow polarization decay, with the delay of the echo given by the delay between fields E_1 and E_2. The response was an echo because, even in a structure with such a narrow absorption feature, the

excitonic response remained inhomogeneously broadened. (The dephasing rate is small compared to the inhomogeneous broadening due to the presence of disorder.) But if the first two incident fields were linearly cross-polarized ($\mathbf{E_1}\perp\mathbf{E_2}$, designated $\text{FWM}_\perp$), the response became a prompt free polarization decay signal with a rapid polarization decay. The electric field polarization dependence of the detected polarization decay was also observed by other groups, and more recent work has shown this behavior to be sample dependent. A more detailed review of this behavior and discrepancies between the observed response and the SBE is provided in the recent work on the determination of the Stoke's parameters by Smirl's group.

There have been several proposed interpretations of these observations. A model considering disorder-induced band mixing accounted well for the transient behavior and differences in dephasing rate for quantum-wells with large inhomogeneous broadening. However, studies in nearly homogeneously broadened quantum-wells suggested that the difference between the transient behavior of the $\text{FWM}_\parallel$ and $\text{FWM}_\perp$ was due to strong Coulomb correlations. Additional studies have also supported the importance of Coulomb interactions on the polarization dependence of the nonlinear signal in GaAs quantum-wells. Other experiments supported an alternative picture that included biexciton states. This model has been successful in interpreting some of the critical observations, including the differences in dephasing rates and signal strengths, the polarization-dependent negative-time-delay signal, the polarization-dependent echo signal, and the quantum beats in differential transmission for oppositely-handed pump and probe beams. Nevertheless, it was clear that additional experimental insight was needed.

Since it is clear that disorder results in considerable complexity, our group chose to investigate the polarization behavior of the nonlinear response in high-quality bulk GaAs. In the three-dimensional system, in contrast to the nearly two-dimensional quantum-well, the SBE indicated that the roles of band-filling and exchange effects were less significant, but that the general behavior was expected to be similar. As in the quantum-well, for which the light-hole-heavy-hole degeneracy is lifted by confinement, in bulk material the application of uniaxial strain also lifts the degeneracy and permits us to selectively study either exciton species.

To understand the origin of the polarization dependence, we must first understand the role of polarization in the original formulation of the SBE. For this, we refer to the energy level diagram in Fig. 1, where the dipole selection rules show that $\sigma_{+(-)}$-polarized light excites $|+1\rangle$ ($|-1\rangle$) excitons. Also shown in Fig. 1 is the standard backward FWM geometry, in which $\mathbf{E_1}$ and $\mathbf{E_2}$ form a grating in the material (ignoring two-photon effects) from which $\mathbf{E_3}$ scatters, producing a phase-matched nonlinear signal field $\mathbf{E_4}$ in the $-\mathbf{k_1}$ direction proportional in lowest order to $\chi^{(3)}E_1^*E_2E_3$. Since linearly polarized light is a linear superposition of left- and right-circularly polarized light, the interaction of linearly co-polarized beams, $\mathbf{E_1}\|\mathbf{E_2}$, with the sample produces *spatially coincident* $|+1\rangle$ and $|-1\rangle$ exciton population gratings, which combined form a net population grating. In contrast, linearly cross-polarized beams, $\mathbf{E_1}\perp\mathbf{E_2}$, produce $|+1\rangle$ and $|-1\rangle$ exciton population gratings spatially 180º out of phase with each other. Thus there is *no net population grating* for linearly cross-polarized fields.

Because the original formulation of the SBE included only static Coulomb and spin-dependent interactions, each of the two circularly polarized components of $\mathbf{E_3}$ was predicted to couple only to the corresponding $|+1\rangle$ or $|-1\rangle$ exciton grating. That is, the SBE predicted that the FWM signal resulted from the separate scattering of the $\sigma_{+(-)}$ component of $\mathbf{E_3}$ from only the $|+1\rangle$ ($|-1\rangle$) exciton grating, respectively. Since these two scattering processes are identical to within a phase factor, the SBE predicted no qualitative difference between the linearly co- and cross-polarized FWM signals. Experimentally, however, the linearly co-polarized signal was often found to be at

least an order of magnitude stronger than its cross-polarized counterpart. More significantly, the results showed that the rate of polarization decay also depended on the relative electric field polarization orientation. These observations provided the first clear indication that the SBE did not provide an adequate vectorial description of optical interactions in semiconductors. During the course of the present program, we identified the physical process responsible for the observed polarization dependence (in bulk GaAs), which we describe below.
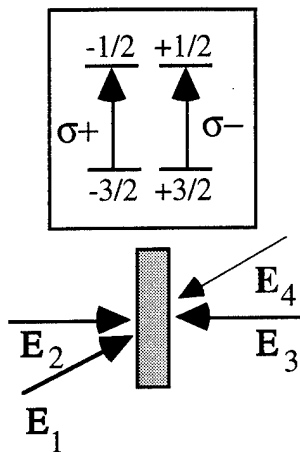

Figure 1. Above: Angular momentum substates of hh exciton with selection rules. Below: Geometry for backward four-wave mixing. The signal field, E_4, is generated by the coherent nonlinear interaction proportional to $E_1*E_2E_3$
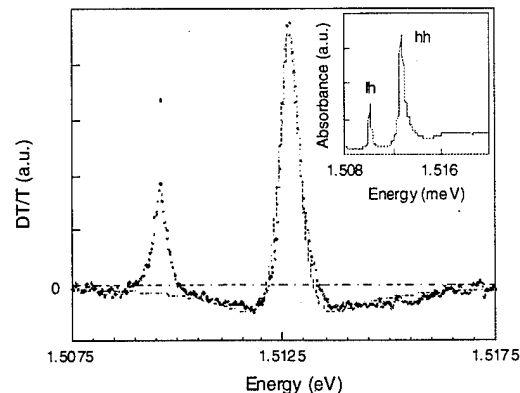

Figure 2 DT spectrum at an exciton density of $3\times10^{15}/cm^3$. The dashed line is the fit discussed in the text. Height is the only free fitting parameter. Inset : Linear absorption of the sample.

To study the origin of the polarization dependence, DT and FWM experiments were carried out at 6 K in a very high-quality homogeneously broadened 200-nm GaAs layer grown by molecular beam epitaxy. Uniaxial strain along the growth direction lifts the degeneracy between the hh1 and lh1 excitons as shown in the inset of Fig. 2. The absorption width is 0.2 meV for the lh exciton and 0.4 meV for the hh exciton.

We first consider the DT data which provide a basis for determining the dominant nonlinearities in the system. Note that assuming a simple harmonic oscillator response, the nonlinear response can be isolated to the oscillator strength, resonance frequency or damping leading to a DT response resembling a Lorentzian lineshape, first order derivative of a Lorentzian lineshape, or second order derivative of a Lorentzian lineshape, respectively. The laser pulses for the DT measurement had an autocorrelation width of 1.5 ps and a spectral width of 4 meV, centered 1 meV below the hh resonance. The probe beam was spectrally resolved with 0.1 meV resolution by an optical multichannel analyzer. The response of the hh is shown in Fig. 2. The DT spectrum of the hh is nearly symmetric and shows only a negligible shift in the exciton energy (less than 0.1 meV). The change in the oscillator strength is determined by the spectral integral of the hh DT response. Phase-space filling makes only a small contribution to the bleaching of the hh resonance as seen in the spectrum of Fig. 2, which has a net area less than 5% of the positive area. The dominant nonlinear optical response comes from changes in the linewidth (i.e., dephasing rate). As described more thoroughly below, this is a significant result: The change in linewidth not only shows that the dephasing rate is density-dependent, as is well-known in both bulk and quantum-

6

well GaAs materials, but also implies that *the nonlinear response is proportional to the effective exciton-exciton collision rate.*

If the DT spectrum is represented by the difference of two Lorentzians, then the zero-crossings in the DT spectra can be used to determine the density-dependent dephasing rate as well as the low-density line width. The obtained EID scattering rate is in general agreement with earlier FWM measurements. We fit the *hh* spectrum in Fig. 2 (dashed line) with no adjustable parameter except the peak height. As seen, the agreement is excellent.
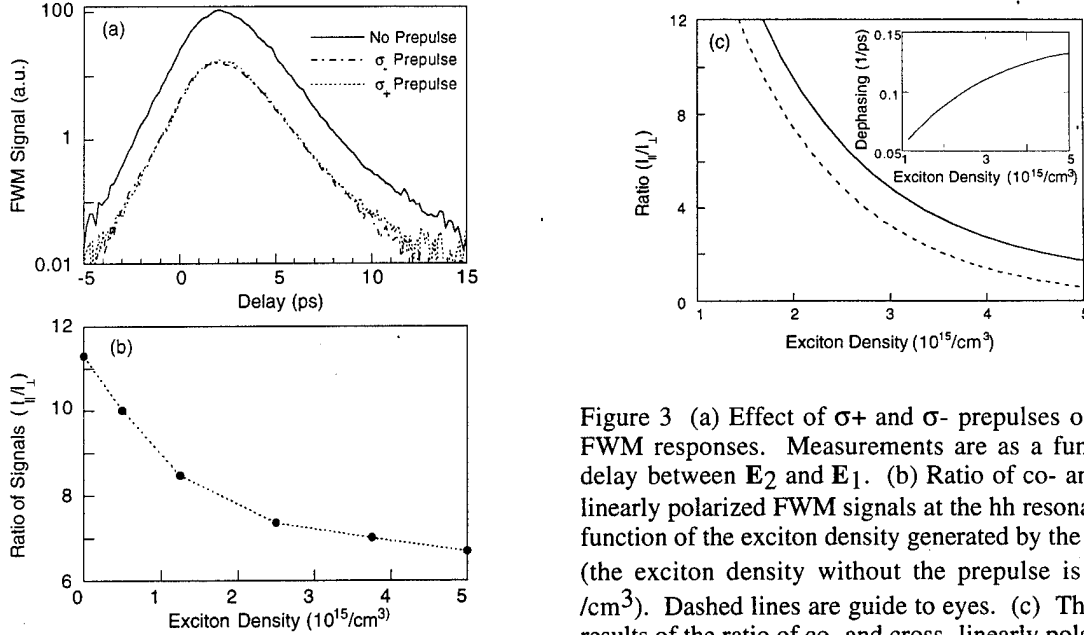

Figure 3 (a) Effect of $\sigma+$ and $\sigma-$ prepulses on the hh FWM responses. Measurements are as a function of delay between E_2 and E_1. (b) Ratio of co- and cross-linearly polarized FWM signals at the hh resonance as a function of the exciton density generated by the prepulse (the exciton density without the prepulse is 6×10^{14} /cm^3). Dashed lines are guide to eyes. (c) Theoretical results of the ratio of co- and cross- linearly polarized hh FWM signals as a function of the exciton density generated by the prepulse. Dashed line is the result (divided by 10) without including exchange interactions. Inset shows the extra dephasing induced by the exciton-exciton interaction.

To examine the dependence of the exciton-exciton dephasing rate on exciton spin, we next examined the self-diffracted FWM signal (in the direction of $2k_2 - k_1$). Figure 3a displays the response at the *hh* resonance with E_1 and E_2 σ_+-polarized. A prepulse with wave vector $-k_2$ arriving 3 ps before E_1 was used to generate excitons ($N = 2 \times 10^{15}$ /cm^3) incoherent with those generated by E_1 and E_2. The incoherent excitons affect the FWM signal only by increasing the dephasing rate, leading to a large reduction (a factor of 6 in Fig. 3a) of the signal strength. From the DT data, the dephasing time (T_2) in the absence of the prepulse was estimated to be 1.7 ps. Since the FWM signals decay with the time constant $T_2/2$ (in this excitation regime), the measurement is pulse-width-limited. In this limit, it is well known that a decrease in T_2 results in a decrease in the time-integrated FWM signal. As shown in Fig. 3a, the presence of a σ_+- or σ_--polarized prepulse results in experimentally indistinguishable reductions in the *hh* signal amplitude, indicating that both $|+1\rangle$ and $|-1\rangle$ excitons are equally effective in reducing T_2 and that *the interaction giving rise to EID is spin-independent.* Spin-flipping of excitons is not important in these measurements since the removal of *hh-lh* degeneracy significantly decreases the exciton spin-flip rate. In separate measurements we have shown that the combined spin and energy relaxation time of the *hh* exciton is longer than 20 ps. While density-dependent exciton dephasing has been reported in earlier DT and FWM measurements in GaAs, the additional dephasing, however, was attributed to spin-dependent exchange effects.

7

Figure 3b displays the ratio, $I_{\parallel}/I_{\perp}$, at the *hh* resonance as a function of the exciton density generated by a prepulse arriving 20 ps before $\mathbf{E}_2$, where $I_{\parallel}$ and $I_{\perp}$ are the FWM signals obtained with $\mathbf{E}_1 \| \mathbf{E}_2$ and $\mathbf{E}_1 \perp \mathbf{E}_2$, respectively. ($\mathbf{E}_1$ and $\mathbf{E}_2$ are linearly polarized.) At a relatively low exciton density, we find $I_{\parallel}/I_{\perp} > 10$. The ratio decreases with increasing prepulse intensities due to saturation of the collision rate.

Analysis shows that the dependence of $I_{\perp}$ on the exciton density is much weaker than that of its counterpart $I_{\parallel}$ because, as discussed above, there is essentially no EID contribution to $I_{\perp}$ aside from contributing to T_2 (since EID is spin-independent). The $I_{\perp}$ signal is affected only by the overall change in the dephasing rate. In contrast, in our parameter regime, the strength of $I_{\parallel}$ is a sensitive function of the *derivative* of the dephasing rate with respect to the excitation density, which is large at low exciton densities but decreases with increasing density due (according to the theoretical model) to screening of the exciton-exciton interaction. In the high-density limit, FWM signals from EID become small with respect to other contributions due to a reduction (saturation) of exciton-exciton scattering cross section. Hence, the ratio $I_{\parallel}/I_{\perp}$ decreases considerably, approaching unity in the theoretical model shown in Fig. 3c (developed by our collaborators at the University of Arizona). Although EID is the dominant nonlinearity and responsible for the density-dependence of the ratio $I_{\parallel}/I_{\perp}$, one must not neglect the importance of exchange effects. We illustrate this with the dashed line in Fig. 3c, calculated for the same parameters as above but with the exchange interaction artificially omitted from the SBE. The result of this demonstration is a large (about ten times) enhancement of the ratio $I_{\parallel}/I_{\perp}$. This underscores the fact that exchange dominates $I_{\perp}$ (as in the original SBE) but only weakly influences $I_{\parallel}$, which is dominated by EID. Therefore the incorporation of EID into the SBE is essential to explain the polarization and density dependence of the FWM signal, but both EID and exchange are necessary for a complete description of the nonlinear response.

II.A.2. NONLINEAR SPECTROSCOPY STUDIES

The measurements described in this section are performed using high resolution frequency domain four-wave mixing with frequency stabilized cw dye lasers. Analysis of the extensive information that can be obtained using this approach to FWM is described in work supported in an earlier AFOSR program.

Biexcitonic contribution to the nonlinear optical response in GaAs:

It has been well established theoretically that the binding energy of biexcitons in semiconductors decreases rapidly with a decreasing ratio of the effective hole mass to the effective electron mass . Hence, the relatively large binding energy of biexcitons in CuCl (with a binding energy $E_B \sim 30$ meV) or CdS and CdSe ($E_B \sim 5$ meV) facilitated the detection and study of these excitations. The existence of biexcitons in GaAs, however, has been much more difficult to confirm because of the small binding energy (theoretical estimation $E_B \sim 0.15$ meV).

Traditionally, investigations of biexcitons were conducted either by two-photon absorption at an energy equal to half of the biexciton energy or by analyzing the excitation density dependence of photoluminescence associated with radiative decay from the biexcitonic state to the free exciton state. Recently, the effects of biexcitons in GaAs quantum-wells, where E_B is enhanced because of confinement, have been studied through the spectral and polarization properties of the nonlinear optical response of the material. The existence of biexcitons in GaAs/AlGaAs quantum-wells was suggested by the temporal oscillation behavior in DT for oppositely-handed circularly-polarized pump and probe beams, as well as in FWM for linearly cross-polarized excitation beams. In a strongly inhomogeneously broadened system, the photon echo was attributed to a two-exciton coherence. The transient FWM response measured at negative time delay, distinct dephasing rate, and alteration in the homogeneity of line broadening detected in transient FWM with different

8

exciton spin characteristics were also attributed to biexcitonic effects. More directly, careful studies of the spectrally-resolved transient FWM experiments have also been able to show a clear contribution from the biexciton resonance. In bulk GaAs, a photoluminescence peak characterized by a superlinear dependence on excitation level was attributed to a biexciton resonance, though the reported binding energy (0.5 meV) was larger than the theoretical estimation.

Using cw polarization-sensitive FWM (refer to Fig. 1 for geometry) in strained bulk GaAs, we have observed polarization-dependent resonances in the nonlinear optical response that are red-shifted with respect to *lh* and *hh* excitonic resonances, respectively (the shift is ~0.2 meV at the *lh*). The spin dependence of this red-shifted signal, the excitation-density-independent value of the red shift and the observation of an induced absorption at a corresponding energy supports the assignment of this behavior to bound exciton complexes, i. e. biexcitons. Measurements of the decay dynamics demonstrate that the response is associated with step-wise excitation, and the red shift corresponds to the binding energy of the biexcitons (~0.2 meV for *lh-lh* and ~1 meV for *lh-hh* complex). Furthermore, decay profiles measured with differential FWM (in the presence of a incoherent pump beam), clearly exhibit evidence of nonlinearities distinct from the excitons and consistent with the assignment of biexcitons.

The polarization dependence of the FWM response was first investigated as a function of the back beam frequency, ω_3, (denoted FWMω_3) with E_1^* and E_2 tuned in resonance with the *lh* excitons (Fig. 4). As shown in Fig. 4 (curve b), the FWM$\omega_{3\parallel}$ shows no frequency shift with respect to the linear absorption (curve a). Such results are consistent with earlier theoretical predictions and experimental reports showing that the Coulomb screening and the exchange interaction give nearly equal but opposite shifts in bulk GaAs. On the other hand, the FWMω_3 spectrum obtained for $E_1 \perp E_2$ (Fig. 4, curve c) clearly reveals a *red shift* and changes in line width with respect to the *lh* and *hh* exciton resonances. (The small resonance at 1.5033 eV saturates easily with excitation density and is believed to be related to impurities.)
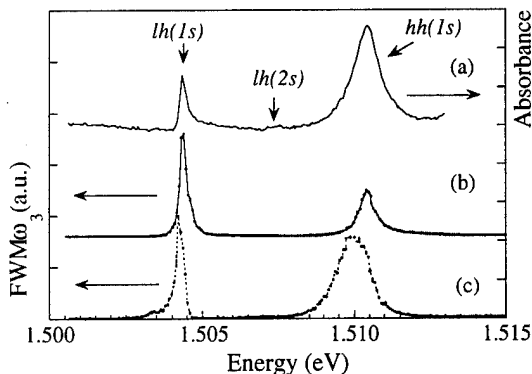

Figure 4. (a). Linear absorption spectrum. (b) FWM$\omega_{3\parallel}$ spectrum. (c) FWM$\omega_{3\perp}$ spectrum. Excitation energy determined by the frequencies of the fields giving rise to $E_1^* \cdot E_2$ is fixed at *lh*(1s) resonance. Inset: backward FWM configuration.

The ratio of the amplitudes between FWM$\omega_{3\parallel}$ and FWM$\omega_{3\perp}$ is ~500:1, this large ratio, however, does not imply an intrinsically weaker DT response. In the cw FWM described here, the signal strength varies as the square of the excitation grating relaxation time. As was discussed earlier, the appropriate time in the FWM$_\perp$ geometry is twice the exciton spin-flip time (~125 ps); while in the FWM$_\parallel$ geometry, the time is mainly given by exciton recombination (~ 0.85 ns) for large grating spacing. Hence, if measurements were made in the transient regime, the strengths of the signals would be comparable.

9

Recalling that only spin-dependent interactions may generate a $FWM_\perp$ signal, a red-shifted $FWM\omega_{3\perp}$ response could, in principle, be due to several effects. For example, exchange effects are well known to lead to a shift in the resonance frequency. This explanation is unlikely, however, since the exchange interaction depends strongly on excitation density while experimentally we find that for excitation densities varying over more than an order of magnitude, the $FWM_\perp$ signal strength is nearly cubic while the value of the red shift remains *constant for the whole range of applied excitation densities*. Alternatively, a Raman-type contribution to the nonlinear response is also a possibility however, such a resonance is determined by the detuning between E_1 and E_2, which is not the case for the present result. We also note that impurity effects could also lead to a shifted resonance (e.g., the FWM peak at 1.5033 eV) though contributions from impurity bound excitations saturate at relatively low excitation density, unlike the primary resonance in curve c. However, the density-independent value of the red shift, the selection rules, and the lack of saturation are all consistent with assigning the red-shifted $FWM_\perp$ resonance to biexcitons.

In the $FWM\omega_{3\perp}$ spectrum (curve c), the absence of a distinct excitonic spin-dependent component can be attributed to two effects: First, the dipole moment associated with the transition from exciton to biexciton is predicted to be "giant" due to the large biexcitonic Bohr radius, hence the biexcitonic nonlinearity is expected to be larger than the spin-dependent component of the excitonic nonlinearity. Second, the binding energy of the biexciton has a value comparable with the line width of the exciton resonance. Hence, the two peaks cannot be well resolved but the whole peak appears at a somewhat bluer position and is asymmetric on the high energy side.

Assuming the $FWM_\perp$ response is due to biexcitons, we consider two excitation pathways: the two-photon coherence and the step-wise excitation. Clarification of the dominant pathway is possible by studying the decay dynamics of the $FWM_\perp$ response. For the two-photon-coherence, the perturbation sequence is:

$$N_g \xrightarrow{\mathbf{E}_2(\mathbf{E}_3)} p_{xg} \xrightarrow{\mathbf{E}_3(\mathbf{E}_2)} p_{bg} \xrightarrow{\mathbf{E}_1^*} p_{bx}, p_{xg}$$

(where g, x, b represent the ground, exciton and biexciton states respectively, and p and N describe the optical polarization and population respectively). The FWM signal arises from the optically-induced quantum coherence, p_{gb}, oscillating in time with frequency $2\Omega - \Omega_b = \omega_2 + \omega_3$ (with resonant excitation) where   is the exciton transition energy and $\hbar\Omega_B$ is the biexciton binding energy, as seen directly in CuCl [105]. For the step-wise excitation, the perturbation sequence is:

$$N_g \xrightarrow{\mathbf{E}_2(\mathbf{E}_1^*)} p_{xg}(p_{gx}) \xrightarrow{\mathbf{E}_1^*(\mathbf{E}_2)} N_x \xrightarrow{\mathbf{E}_3} p_{bx};$$

The FWM signal is diffracted from the population gratings excited by $\mathbf{E}_1^*$ and $\mathbf{E}_2$. The contribution due to the back grating ($\mathbf{E}_3\mathbf{E}_1^*$) is experimentally verified to be negligible because the excitons quickly diffuse out of the tightly spaced grating.

The contribution of the two-photon-coherence to the FWM response can be identified by using oppositely circularly polarized $\mathbf{E}_1$ and $\mathbf{E}_2$ beams, for which a pure temporal modulation of p_{gb} (no population grating) is built up when $\mathbf{E}_3$ has the opposite handedness as $\mathbf{E}_1$. The validity of this method is, however, limited by the symmetry of the system which unfortunately often deviates from a perfect cubic symmetry. The second means of detecting the coherent two-photon excitation is to use linearly polarized $\mathbf{E}_2$ and $\mathbf{E}_3$ beams and tune the frequency of $\mathbf{E}_1$; in this case, two strong peaks are expected, based on the perturbation sequence presented above. Observation of such a double peak was reported for transient FWM in GaAs QWs. In our frequency domain

10

measurement, however, tuning $\mathbf{E}_1$ resulted in only a single peak centered at $\omega_1=\omega_2$, corresponding to that expected for the step-wise excitation path. The width of the $\text{FWM}_\perp\delta$ profile measures the decay rate ($\sim 125 \text{ ps}^{-1}$) of the excitation transfer between the $\sigma-$ and $\sigma+$ exciton gratings generated by $\mathbf{E}_1^*$ and $\mathbf{E}_2$, as was discussed earlier. The absence of a double peak and the zero base line of $\text{FWM}_\perp\delta$ indicates that the two-photon coherence is negligible in $\text{FWM}_\perp$. Direct determination of the two-photon-coherence is possible, however, in the time domain, as we will propose it in the next section. (Note: The cw response of the two-photon coherence is usually weak because the signal varies as inverse squared of the two-photon dephasing rate, whereas the stepwise contribution varies as the inverse squared of the exciton decay rate, usually a much smaller number.)

Based on the above analysis, we tentatively assign the $\text{FWM}_\perp$ resonance to a step-wise excitation of the biexciton; the red shift measures the binding energy of the two-exciton state, which is ~0.2 meV for *lh-lh*, which is very close to the theoretical estimation of the binding energy of biexcitons. With excitation beams creating *lh*-excitons, the red shift of $\text{FWM}\omega_{3\perp}$ at the *hh* gives the binding energy for *lh-hh* two-exciton state. The larger binding energy for the *lh-hh* two-exciton state (~ 1 meV) compared to that for *lh-lh* state is believed to be due mainly to the difference in the effective masses of the *lh* and *hh*. It is noteworthy that stress present in the sample results in anisotropic effective masses of the *lh* and *hh*. This anisotropy in effective masses can lead to larger values of binding energy than that calculated using the isotropic approximation, since the two excitons can be bound along the heavy axis. In addition, the *lh-hh* complex must consist of excitons of parallel spins, while the *lh-lh* complex must have anti-parallel spins in order to satisfy the Pauli exclusion principle. Therefore, the binding energy may also be influenced by spin interactions, though the effect is expected to be small because of the small effective g-factor of excitons.

The assignment of a biexcitonic state in our sample is also supported by DT measurements, where formation of biexcitons results in an increase in absorption. Curve fitting and systematic studies of the intensity dependence show that, in addition to the component resonant with the exciton, the DT contains an excitation-energy independent red-shifted component with a shift comparable to that observed in FWM. The DT component resonant with the free excitons is dominated by EID except at very low excitation density where an induced absorption is observed. Details about this feature are discussed in the following section.

Observation of the Ultrafast Two-Photon Coherent Biexciton Oscillation in a GaAs/AlGaAs Multiple-Quantum-Well

In related experiments, we looked for direct evidence of the nature of the quantum coherence of the biexciton excited directly by two-photon excitation. As identified above, the biexcitonic nonlinear response in FWM arises from two competing and fundamentally different excitations paths which have analogs in the theory of three-level atoms. The path that dominates in studies of biexcitons in long time scale measurements (e.g., luminescence) is the incoherent stepwise generation of biexcitons excited directly from a population of excitons. The other path excites biexcitons through the non-radiative two-photon coherence induced between the ground and biexciton state which oscillates in time at the biexciton frequency. This path becomes important for time scales comparable to the two-photon coherence dephasing time. Here, we qualitatively demonstrate the unique features of the two-photon coherence path in GaAs by using heterodyne FWM to identify the ultrafast 770-Terahertz two-pohton coherence oscillation. The utility of interferometric measurements in the vicinity of a single-photon resonance has been established in recent measurements of nonlinear phase shifts and pulse distortions in GaAs MQWs. Identification of the two-photon coherence, however, requires a very different interferometer

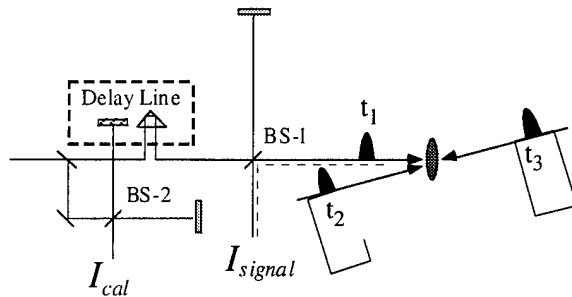specifically designed for investigating two-photon resonances, as described below and shown in Fig. 5.

Figure 5: Geometry of the phase-conjugate Michelson interferometer.

Detecting the two-photon coherence requires careful discrimination of several signals, especially contributions from two-level FWM, including concomitant exciton-exciton interactions (EEI) which partially relax nominal time-ordering. In phase-conjugate FWM, two pulses, $E_1(\omega, \mathbf{k}_1)$ and $E_2(\omega, \mathbf{k}_2)$, interact with the sample at times t_1 and t_2, respectively, to produce an excitation grating. A third pulse, $E_3(\omega, -\mathbf{k}_2)$ diffracts from the grating to produce a signal polarization propagating in the background-free direction $-\hat{\mathbf{k}}_1$. Except as noted, we take the arrivals of E_2 and E_3 to be simultaneous, $t_3 = t_2$, a time $\tau \equiv t_2 - t_1$ after E_1. The appearance of a signal for negative delays, $\tau < 0$, is evidence of EEI such as local fields, excitation-induced dephasing, and (in three-level systems) the two-photon coherence, which has no grating analogy. In the data below, we demonstrate the ultrafast two-photon coherence oscillation and present polarization-dependent data to assess the influence of non-two-photon coherent EEI on the experiment.

The density matrix representation above illuminates key features of the stepwise and two-photon coherence paths. A close inspection of the two-level, stepwise,. and two-photon coherence paths reveals a crucial distinction. The population which contributes to the two-level and stepwise paths, is quasi-stationary, but the electronic phase of the two-photon coherence evolves via the ultrafast quantum coherence, p_{bg}, after the arrival of the first two pulses. The two-photon coherence is independent of any exciton population. Although the two-photon coherence is nonradiative (i.e., direct biexciton creation is not dipole-allowed), the phase of the two-photon coherence is sampled by E_1 and impressed upon the radiative signal polarizations, p_{bx} and p_{xg}. The two-photon coherence can therefore be extracted interferometrically by heterodyne detection. If the FWM signal is mixed with a suitable local oscillator, E_r, the total signal measured by a slow detector is modulated at the two-photon coherence frequency with respect to delay τ .

We employ the femtosecond phase-conjugate Michelson interferometer in Fig. 5 to observe the two-photon coherence as a function of the delay, τ. Since this method detects a phase shift, not the envelope of the emission, pulses need not be short on this time scale, and we use picosecond pulses to avoid hh-lh beats. A single synchronously pumped mode-locked dye laser provides approximately Gaussian pulses with 4 ps autocorrelation width and 0.7 meV bandwidth tuned to the $hh1$ exciton resonance. The MBE-grown sample contains ten 100-Å GaAs wells separated by 100-Å $Al_{0.3}Ga_{0.7}As$ barriers. The absorption line width is 1.0 meV, and the Stokes shift is 0.3 meV. The main interferometer (using BS-1 in Fig. 5) is a modified Michelson design; the sample acts as a phase-conjugate mirror forming one arm of the interferometer. The delay line is dithered

12

over several optical cycles using a piezoelectric element. This special geometry, in which E_r and E_1 are delayed in equal increments assures that the interferogram is sensitive only to the delay, $\tau = t_2 - t_1$, and not to the time interval, $t_1 - t_r$. In contrast to earlier interferometric studies which were not sensitive to the temporal oscillation of the two-photon coherence, this geometry produces no interference fringes near the laser frequency, independent of the origin of the nonlinear response. An auxiliary Michelson interferometer (using BS-2) produces conventional laser fringes to simultaneously calibrate the delay line.

A typical single scan is displayed in Fig. 6, with solid lines to guide the eye. The scatter is due to small laser frequency instabilities affecting the FWM signal. The (approximately) two-to-one ratio between the signal and calibration periods is apparent, and ensemble averaging gives a beat period of approximately 1.3 fs, corresponding to a 770-Terahertz two-photon coherence oscillation. The 10% uncertainty precludes a measure of the biexciton binding energy, which would require precision of 0.03%. As indicated above, interpretation of this data in terms of the two-photon coherence oscillation requires care to eliminate potential alternative origins of the oscillation. These signals arise from "ordinary" interferometry of two-level FWM, rather than from the electronic phase of the two-photon coherence.
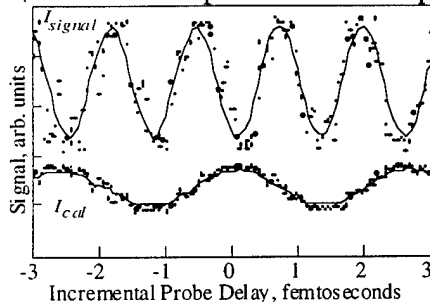

Figure 6: Typical simultaneous scans (offset for clarity) of signal and calibration interferometers for $\tau \approx -3 ps$. Lines are guides to the eye. The approximate 2:1 ratio of the two-photon coherence and laser (resonant with the exciton) is clear.
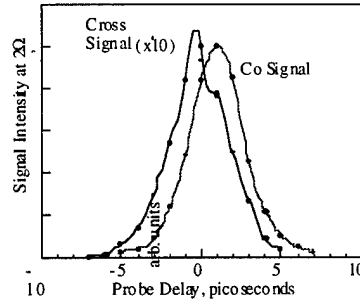
Figure 7: Intensity of the approximately $2\Omega_{eg}$ oscillation for co- and cross-polarized fields versus delay, $\tau = t_2 - t_1$. The cross-polarized signal favors negative delay, as expected for the two-photon coherence. Lines are guides to the eye.

Finite pulse width effects may be significant if the pulse width is comparable to the FWM decay time, as in our experiment. But even for moderately pulse-width-limited data, the non-two-photon coherence signals favor positive rather than negative delay. Moreover, the signal for $\tau > 0$ has a strong polarization dependence in GaAs MQWs and is substantially reduced for E_1 cross-linearly polarized with respect to both E_2 and E_3, $E_1 \parallel E_r \perp E_{2,3}$. In Fig. 7 we plot the Fourier spectral power density of the heterodyne signal in the vicinity of Ω_{bg} for both co- and cross-linearly polarized configurations, as a function of delay, τ. For cross-polarized fields, the oscillation favors negative delay, as expected for the two-photon coherence. This observation strongly supports the interpretation that the negative-delay signal is in fact the two-photon coherence.

For completeness, we note that the spectrally resolved FWM reveals two peaks: a "free" exciton peak and a Stokes-shifted peak, similar to an earlier observation. The observation of the two-photon coherence oscillation shows the presence of the nonradiative biexciton coherence and demonstrates its importance for observation time-scales comparable to the two-photon coherence dephasing time. Continued refinement of techniques to quantitatively characterize the two-photon coherence oscillation will enable measurements of coherent non-radiative biexciton dynamics not accessible in conventional optical measurements such a luminescence, where the relative

contribution of the two-photon coherence is generally negligible compared to the incoherent SW contribution.

Nonlinear magneto-optical properties of GaAs: Magnetic Freezeout

Further studies of the fundamental nonlinear optical response were made in the presence of a moderate magnetic field. Magnetic fields significantly modify the optical and electronic properties of semiconductors. In a direct-bandgap material like GaAs, the Coulomb interaction between electrons and holes leads to a strong excitonic optical resonance just below the bandgap. However, even modest magnetic fields result in the appearance of strong Landau resonances, overcoming effects due to Coulomb coupling. While there has been considerable effort to understand the response in quantum-well systems, much less is known about the nonlinear magneto-optical behavior in bulk semiconductors. Using high-resolution nonlinear laser spectroscopy, we find that the application of magnetic fields causes a major enhancement of the nonlinear optical response in FWM. The enhancement is a direct result of magnetic freeze-out of the excitons due to field induced localization, which causes a reduction in exciton mobility and the corresponding grating relaxation rate. Our measurements, based on the third order susceptibility, $\tilde{\chi}^{(3)}(\omega_4 = \omega_1 - \omega_2 + \omega_3)$ with nearly degenerate and resonant frequencies, demonstrate that the nonlinear response is dominated by Coulomb interactions leading to strong inter-Landau level coupling.

The experiments were performed using the same phase-conjugate FWM geometry as shown in the inset of Fig. 1, and again frequency-stabilized lasers are used. In the simple two state model, two nearly degenerate cw fields, $E_1(k_1, \omega_1)$ and $E_2(k_2, \omega_2)$ ($\omega_1 \approx \omega_2$), intersect in the sample separated by a small angle θ, producing a traveling-wave modulation of the absorption and dispersion with period $\Lambda = \lambda/2 \sin(\theta/2)$; λ and θ are the wavelength and angle, respectively, in the material. The resulting grating is probed by a third beam, $E_3(-k_2, \omega_3)$, giving rise to a coherent signal proportional to $|\chi^{(3)}|^2$ in the direction $-k_2$. All three incident beams are independently frequency- stabilized with a linewidth of 1 MHz (5 neV). As reviewed here, spectral information can be obtained as a function of the frequency of any one of the three incident beams; specifically, tuning ω_3 measures the spectral response induced by E_1^* and E_2, which gives information on the quasi-equilibrium excitation population produced by spectral diffusion and coupling between excitations at different energy (e.g., inter-Landau level coupling). In the presence of inhomogeneous broadening (with no coupling between the different frequency groups), this response will also show spectral hole burning. Tuning $\delta = \omega_1 - \omega_2$ probes the energy relaxation rate of the excitation grating, γ_{rel}. Here $\gamma_{rel} = \gamma + \Gamma_d$, where γ is the inverse of the effective lifetime of individual excitations, and $\Gamma_d = 4\pi^2 D/\Lambda^2$ is the addition to the decay rate due to spatial diffusion of excitons with diffusion coefficient D. In the case of an single isolated excitonic response and with γ_{rel} much smaller than the dephasing rate γ_{ph}, the FWM lineshape (as a function of δ) is a Lorentzian with a linewidth determined by γ_{rel}. When there exists more than one excitation grating (e.g. coupling between excitons at different energy states), all gratings contribute to the nonlinear response with characteristic decay rates. The FWM profile is then a sum of multiple complex Lorentzians.

The sample is identical to that described above and the linear absorption spectrum of the sample at 6 T is shown in the upper part of the Fig. 8a. The data reveal a rich structure due to the combined effects of strain and magnetic field. In the presence of a magnetic field, *hh* and *lh* excitons form an incommensurate series of Landau levels, because of the different effective masses. In the absorption spectrum, some forbidden transitions become observable due to the

14

lowering of symmetry produced by the strain. The nonlinear optical response with degenerate frequencies is displayed in the lower part of the Fig. 8a. The data show much less structure than the corresponding linear absorption and consequently the regular pattern due to *hh* Landau level resonances is clearly evident. The relative contribution of the remaining transitions is reduced due to differences in the associated transition moments and relaxation rates. This behavior is specific to cw FWM spectroscopy (or transient FWM where the pulsewidth is longer than all relaxation times in the system) ,where the strength of the relative signal varies as $\mu^8/\gamma_{ph}^4\gamma_{rel}^2$, as opposed to linear absorption which varies as μ^2/γ_{ph} (μ is the transition moment.).
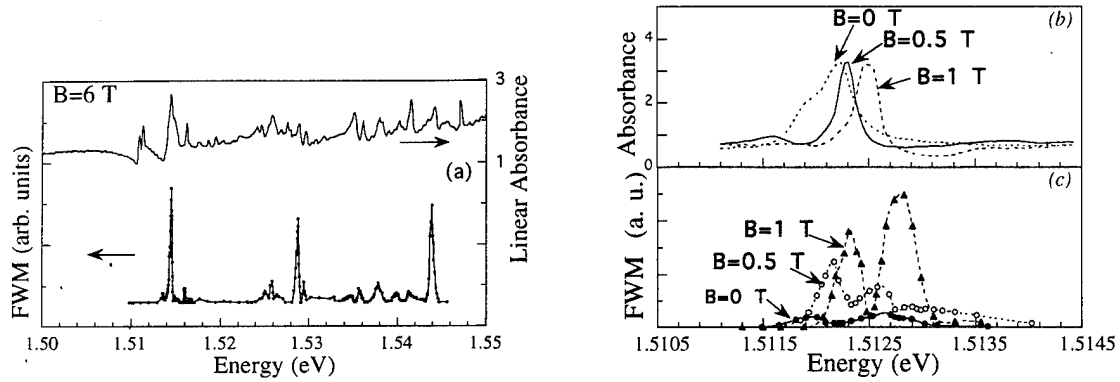

Figure 8. (a) Comparison of linear absorbance and frequency degenerate FWM. (b) Linear absorption spectra and c) Degenerate FWM spectra of the *hh*(1) resonance.

Figure. 8c shows a significant enhancement of the nonlinear response of the *hh*(1) resonance with increasing magnetic field. Here *hh(n)* represents the exciton associated with the *n*-th Landau level of the conduction electron and the heavy hole. The frequency shift in the linear absorption spectrum with increasing field (Fig. 8b) is due to the diamagnetic term. When the applied magnetic field increases from zero to 1 T, the degenerate FWM signal increases by an order of magnitude while the dipole moment (reflected in the linear absorption spectrum) remains nearly constant. (We note that the dip present in the nonlinear response is due mainly to the strong absorption; however, for B≥1 T the dip persists after this correction).
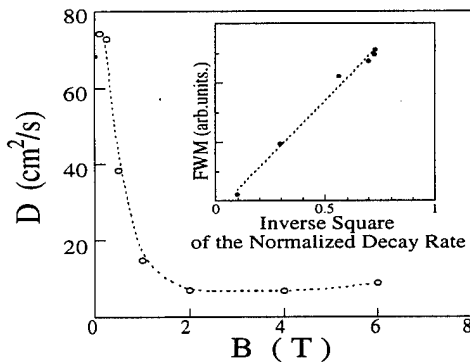

Figure 9. Dependence of diffusion coefficient on magnetic field. Inset: Frequency degenerate FWM versus inverse square of the normalized decay rate $(\gamma_{rel}/\gamma)^{-2}=(1+4\pi^2D/\Lambda^2\gamma)^{-2}$

To understand this enhancement, we recall from above that while the relative linear and nonlinear response both depend on the dipole moment and γ_{ph}, the nonlinear response also

15

depends on $\gamma_{rel}^{-2} = \left(\gamma + 4\pi^2 D/\Lambda^2\right)^{-2}$. Hence for a constant Λ, a decrease in D will result in an increase in the FWM response. The diffusion coefficient D can be extracted accurately by measuring the dependence of γ_{rel} on Λ, which varies as a function of angle between the $\mathbf{E_1}$ and the $\mathbf{E_2}$ beams. Figure 9 shows the measured diffusion coefficient, which decreases with increasing B. Such behavior has been predicted in studies of exciton transport in magnetic fields. The increasing field decreases the spatial extent of the exciton wave function. This enhances the likelihood of localization on defects and impurities (magnetic freeze-out) which decreases the mobility. Experimental evidence for this effect was recently reported in germanium. In GaAs, the above measurements show that the diffusion coefficient, D, of $hh(1)$ excitons is reduced by a factor of 5 at fields as low as 1 T. Consequently, the FWM response at a fixed Λ is expected to depend linearly on the inverse square of the normalized decay rate, $\left(\gamma_{rel}/\gamma\right)^{-2}$. The inset in Fig. 9 shows the predicted linear dependence for magnetic fields ranging from 0 to 6 T. Thus we conclude that the reduction in mobility of magneto-excitons (i.e., magnetic freeze out) is the origin of the enhancement in the nonlinear response.

In quasi-two-dimensional systems, it has been shown that exciton-exciton coupling via Coulomb screening is important only for excitons belonging to different Landau levels, and that the nonlinear spectrum depends sensitively on the excitation energy. From our results however, it follows that the nonlinear response of excitons in bulk GaAs differs from that in quantum-wells. Fig. 10 shows that the spectrum of the nonlinear response, obtained by tuning ω_3 for two different excitation frequencies, is nearly *independent of the excitation frequency.*

In general the spectral response obtained by tuning ω_3 is used to determine the quasi-equilibrium distribution of excitations. Our data suggests that a significant fraction of the generated excitons relax to the lowest energy state, $lh(1)$, prior to recombining and hence creates an easily observable nonlinear response. The signal at the $lh(1)$ state is not observable in Fig. 8 (FWM with *degenerate* ω_i) due to its small absorption coefficient and correspondingly small excitation density (note that the FWM response is proportional to the *square* of the excitation density). However, as shown in Fig. 10b, when the excitation is at 1.5145 meV (the $hh(1)$ state) a strong resonant response is observed at 1.535 eV (the $hh(2)$ state) even though no excitons are expected for this excitation energy and temperature ($k_B T \sim 0.4$ meV). Hence, the nonlinear response at $hh(2)$ is the result of Coulomb coupling between $hh(2)$ excitons and those at the $n=1$ Landau level. Accordingly, inter-Landau level coupling must be a dominant mechanism of the nonlinear optical interaction.
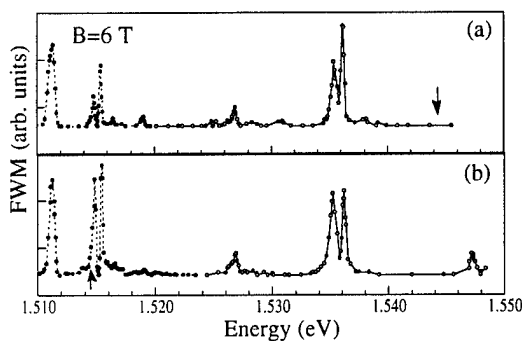

Figure 10. Spectral response measured as a function of ω_3 with $\omega_1 = \omega_2$ tuned to the energies indicated by the arrows.

Further understanding of the nonlinear response and a determination of the relative importance of inter-Landau level coupling is obtained by additional studies of the FWM lineshapes as a function of δ for the $hh(1)$ and $hh(2)$ exciton with ω_1 and ω_3 *resonant with hh(n)*. The details are provided in the attached reprints (see appendix). The primary observation is that the nonlinear

response at a given $hh(n)$ is due to excitons at that energy level as well as inter-Landau level coupling effects (due to excitons located at some other energy). The FWM response is given by two Lorentzians (each with a line width given by the decay rate of the corresponding excitation). A full analysis of the data (see appendix) shows that it is likely that the interactions between the excitons from the same Landau level and that between excitons from different Landau levels arise from the same Coulomb interaction .

Studies of Exciton Motion in GaAs: Non-Diffusive Transport

Optical grating experiments have been shown to be a powerful probe of carrier diffusion. In these experiments, two beams interfere in a material, forming a grating which is probed by a third beam. The decay of the optically-created population grating occurs through many channels, such as recombination (γ_{rec}) and spatial diffusion. As discussed above, for diffusion independent of position and concentration, the decay due to spatial diffusion is governed by Fick's Law and the diffusion coefficient (D) is extracted by measuring the grating decay (γ) versus the grating spacing

(Λ), with $\gamma = \gamma_{rec} + \dfrac{4\pi^2 D}{\Lambda^2}$. In the study of exciton motion in semiconductors and molecular crystals, it is usually assumed that the mean free path is sufficiently short compared to the relevant length scale that diffusive behavior, governed by Fick's Law, is expected. However, it has been found by our group that in high-quality GaAs at low temperatures (< 30 K) the apparent momentum scattering rate is sufficiently reduced to lead to a mean free path on the order of the observed length scale (< 10 µm) and *non-diffusive behavior* is observed (through a sub-quadratic dependence of grating decay rate on $1/\Lambda$) due to near ballistic motion.
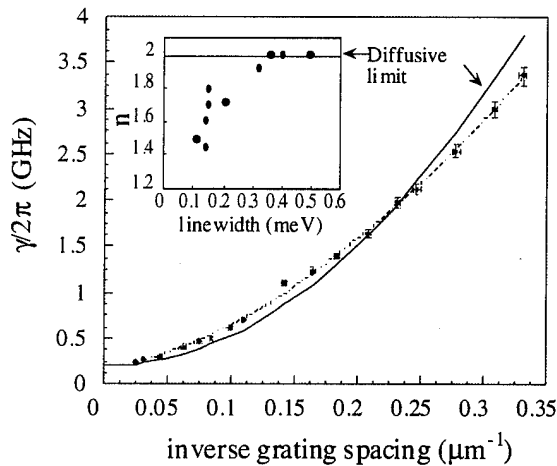

Figure 11. Decay rate of the optical grating signal ($\gamma = \gamma_{rec} + \gamma_{mot}$), as a function of $1/\Lambda$. Data taken at the lh(1s) exciton in GaAs at 4 K with an exciton density of 8 x 10^{14} cm^{-3}. Dashed line: the illustrative fit mentioned in the text with n=1.6 (non-diffusive behavior). Solid line: a quadratic fit, shown for comparison. Upper inset: dependence of the exponent, n, on the momentum scattering rate as indicated by the absorption linewidth (HWHM). Note the transition to diffusive behavior (n=2) for larger linewidths (scattering rates).
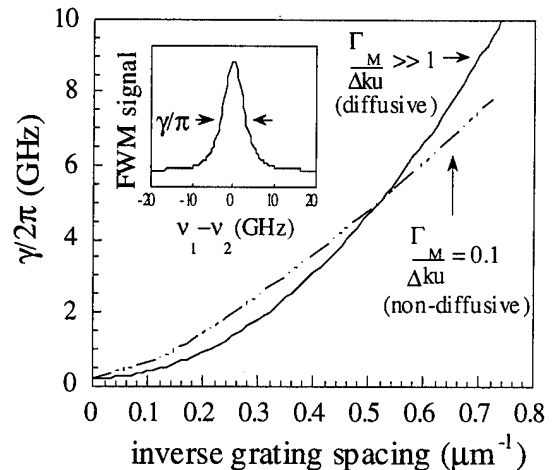
Figure 12. Decay rate of the optical grating as a function of $1/\Lambda$, predicted by a solution of the quantum transport equation, with $\Gamma_m/\Delta ku = 0.1$ (dashed line). Solid line shows the a quadratic dependence in the diffusive limit. Inset: Lineshape predicted in cw FWM for $\Gamma_m/\Delta ku = 0.1$ (nominally Lorentzian, indicating exponential decay).

17

Figure 11 shows the decay rate of the grating taken at 4 K at the lh(1s) exciton resonance as a function of $1/\Lambda$, which is clearly sub-quadratic, indicating non-diffusive behavior. An illustrative fit of $\gamma=\gamma_{rec}+B(1/\Lambda)^n$ is made of the data in Fig. 11, with $n=1.6$. An exponent of $n=2$ indicates diffusive behavior. As shown in the upper inset of Fig. 11, as the momentum scattering rate increases (for example, by increasing the temperature) there is a transition in behavior from non-diffusive ($n<2$) to diffusive ($n=2$).

An exact treatment of momentum-changing collisions in the quantum transport equation accounts for many aspects of the observed data. The critical parameter is the ratio of the momentum scattering rate, Γ_m, to the inverse transit time across a grating spacing, Δku, where u is the mean exciton velocity and $\Delta k=|k_1-k_2|$. When $\Gamma_m \gg \Delta ku$, the solution takes the form given by the Fick's Law description. However, when $\Gamma_m < \Delta ku$, the solution shows a nearly exponential decay with a *sub-quadratic* (non-diffusive) dependence on $1/\Lambda$, in excellent agreement with experiment. This can be seen Fig. 11, in which, for a ratio of $\Gamma_m/\Delta ku = 0.1$, the dependence of the grating decay on $1/\Lambda$ is shown to be highly non-quadratic.

Since the nature of exciton motion is determined by the momentum scattering rate, the non-diffusive behavior is a sensitive probe of the amount of momentum scattering occurring in the system. Surprisingly, our data shows that while exciton scattering due to phonons or disorder leads to both dephasing and changes in the apparent exciton momentum, exciton-exciton scattering, in fact, appears to lead only to dephasing. This observation leads to questions of the fundamental relationship between dephasing and momentum scattering.

Nonlinear Optical Response of the Lowest Energy Excitons in GaAs

As indicated above, it is now well-known that at high density near the band edge in bulk GaAs, phase space filling and screening dominates. At moderate densities excitation-induced dephasing (EID) becomes a major source of nonlinearity as we discussed as well as possibly biexcitons. We find, however, that below exciton densities of about 3×10^{14} cm^{-3} a well-defined transition is observed from behavior dominated by EID to a completely different nonlinear response characterized by induced absorption, spin-dependent interactions, and an excitation-induced line-narrowing (EIN).

Figure 13 shows the cw differential transmission (DT) response showing induced absorption across the whole exciton line at the lh(1s) resonance *which grows superlinearly* with excitation density. This behavior is unexpected in the context of the semiconductor Bloch formalism for these systems and is indicative of a nonlinear response involving *multiple* photons. Time-resolved DT reveals that this response is immediate (within 200 fs resolution). The fact that the response is immediate, has a decay time comparable to the free exciton (≈ 2 ns), is *resonant* with the exciton, and is qualitatively the same for several samples (with different strain and luminescence characteristics) suggests that this behavior is intrinsic. Polarization-sensitive FWM measurements show that the behavior derives nominally from spin-dependent interactions in accordance with the dipole selection rules.

In the same regime, the 2s states also show a strong nonlinear response which indicates an excitation-induced line-narrowing, as shown in Fig. 14. The inset in Fig. 14 shows the standard lineshape expected in transmission for a harmonic oscillator where the dephasing is given by $\gamma = \gamma_o - \beta I$, with $\beta>0$. This observation, coupled with the transition at higher densities to behavior dominated by an increase in dephasing (EID), raises questions on the fundamental mechanisms of the dephasing at these densities.

18

The observation of a multiphoton response at low densities indicates behavior (though barely visible in the linear response) which has yet to be understood. In the standard formalism, it is expected that at these densities the nonlinear response should be third-order and linear with any one of the excitation fields. Currently, a model based on collective effects (excitation-induced enhancement of excitonic oscillator strength) is being considered.
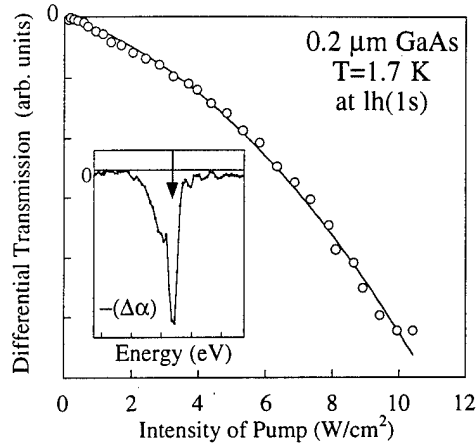

Figure 13. Dependence of DT signal at lh(1s) exciton on pump intensity, showing superlinear growth. Fit is a sum of linear and quadratic terms. Inset: Spectrum of lh(1s) DT, showing complete induced absorption. Arrow indicates position of lh absorption resonance.
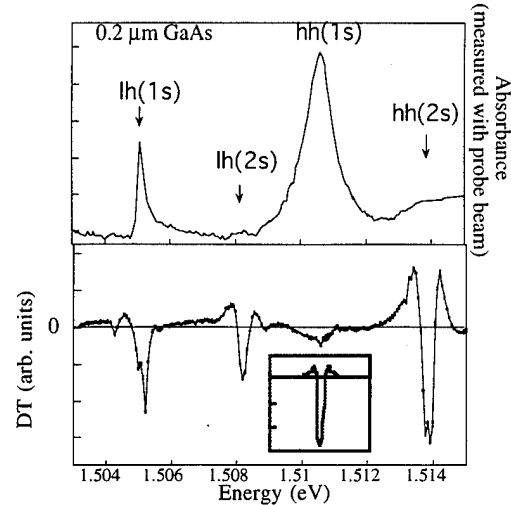
Figure 14. Top: Typical absorption spectra. Note non-Lorentzian lineshape at lh(1s), possibly indicating polariton effects. Bottom: DT spectrum at an excitation density of approximately 5×10^{13} cm^{-3}, showing strong EIN behavior at 2s states. Note also complete induced absorption at hh(1s). A corresponding signal is detected at these resonances in FWM. Inset: Lineshape predicted for EIN.

Polarization Transfer

Ultrafast coherent optical spectroscopy is a valuable technique for investigating the dynamics of various physical phenomena in semiconductors, including exciton dephasing, scattering, and phonon-exciton interaction. In many of these approaches (e.g., four-wave mixing) the polarization of the incident and emitted fields is important for interpretation of the data. An understanding of the related selection rules is essential. Most experiments assume the validity of the circularly-polarized selection rules or at most assume a small linear birefringence that just changes the polarization of the radiated field with respect to the excitation field. In the present experiment we examine the free polarization decay and show that in general this assumption is inappropriate; even weak biaxial strain leads to sufficient symmetry breaking that the polarization of the emitted field differs from the incident field and leads to changes in the temporal evolution of the so-called quantum beats.

Free polarization decay is a phenomenon that occurs when a transient coherent optical field induces a resonant electronic coherence aligned with the field which oscillates at the natural frequency. The induced polarization gives rise to radiation that is phase matched in the direction of propagation of the incident field. Electronic dephasing results in a loss of coherence producing an exponential decay of the macroscopic polarization and radiated field. In a system with axial symmetry, the polarization of the radiated and excitation fields coincide.

19

The experiment is performed in a high quality GaAs material at 4K. The sample is excited by a 100-130 fs pulse of linearly polarized light tuned between the light hole and the heavy hole excitonic resonances. The coherent emission is polarization analyzed and time resolved or sent to a spectrometer. The polarizer analyzes for emission that is co-polarized or cross-polarized relative to the excitation beam.

The results are shown in Fig. 15 which shows the temporal evolution for the two polarizations. The co-polarized signal shows the expected behavior of a double resonance system; a sharp peak at t=0 due to the instantaneous response of the material and the exponential free polarization decay modulated by an interference between the two resonant frequencies. In contrast, the cross-polarized emission is (approximately) 5% of the co-polarized field indicating a significant failure of the angular momentum selection rules. (Values as large 10% have been observed). The temporal evolution differs appreciably from the co-polarized signal, as seen most clearly in the π-phase-shift of the light-hole-heavy-hole beating. The signal at t=0 has the same magnitude as that at later times showing that the *off-resonance* birefringence is much smaller than the *on-resonance* contribution.

The above behavior is in quantitative agreement with the calculated effect of biaxial stress, inherently present in these materials and enhanced during the etching and mounting process. We performed a calculation based on the well-known deformation Hamiltonian for biaxial stress. The results are in excellent agreement with the data, as shown in Fig 16. The in-plane stress mixes the light hole and heavy hole bands at k=0 causing a change in the oscillator strength of the interband transitions. The mixing is mainly between these two bands so that the variations of the oscillator strength in the light hole and heavy hole resonance have the same magnitude and opposite sign. A consequence of this is the polarization dependent π-phase-shift in the interference between the light hole and heavy hole. This model is general and applies to any band-mixing mechanism and adds a new element to the interpretation of the polarization based transient experiments. We note that the data has been well reproduced in all samples we examined including a 100 A multiple GaAs/AlGaAs quantum well where the effects seen are at least as important as in the bulk material.
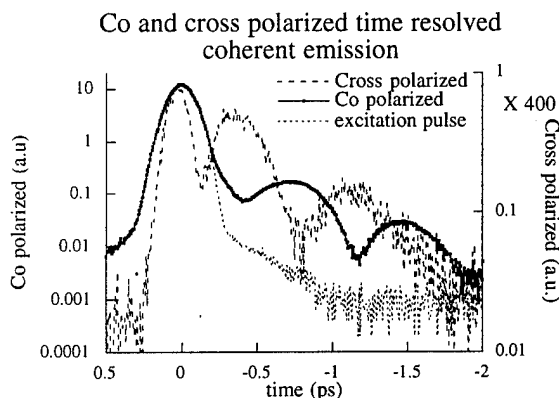
Figure 15. The data shows the time-resolved data for the co (full line) and cross polarized (dashed line) coherent emission.

Figure 16. The time evolution of the co- (full lines) and cross-polarized (dashed lines) coherent emission calculated for a standard set of material parameters.

II.A.3. QUANTUM OPTICAL STUDIES OF GaAs HETERO-STRUCTURE LASERS

Photon-number squeezed light (also known as amplitude squeezed or sub-Poissonian light) is characterized by an uncertainty in the photon-number operator that is below the Heisenberg

20

uncertainty limit for conjugate variables, i.e. for the photon-number, n, $\langle \Delta n^2 \rangle \le \langle n \rangle$.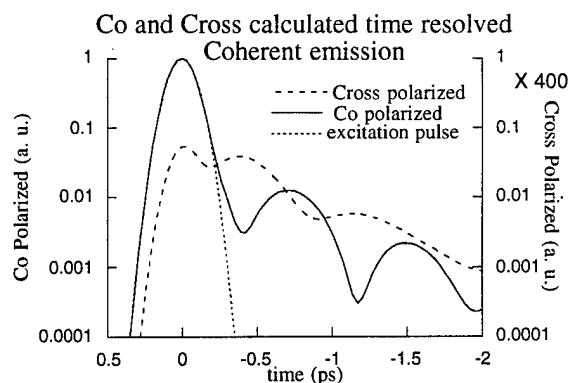 Such a reduction is allowed by the Heisenberg uncertainty principle provided that a corresponding increase in noise above the uncertainty limit is experienced by the appropriate conjugate variable, which in this case is the quantum phase operator. An optical coherent state, which is well described by semi-classical optics, is a minimum uncertainty state where the photon-number fluctuations are at the semi-classical shot-noise limit (SNL), i.e. Poisson distributed noise. Squeezed states of light, characterized by the noise variance of at least one observable below the Heisenberg limit, have properties that can only be described by quantum electrodynamics theory. The Fock state, for example, is the ultimate limit to photon-number squeezing, $\langle \Delta n^2 \rangle = 0$. It is predicted to have zero mean field with a non-zero intensity. No classical analog of this state exists. Quadrature squeezing, which corresponds to reduction of the fluctuations on one field quadrature below the Heisenberg limit, is another common form of non-classical light, especially interesting for generating squeezed vacuum states. In contrast to number-state squeezing, squeezing in a field quadrature is limited due to the energy requirements on the increasing uncertainty of the conjugate field quadrature.

Recent achievements in the development of non-classical sources has allowed for the application of squeezed light to problems of both fundamental and practical importance. Progress in the generation of squeezed light from semiconductor sources has had an impact both on the study of amplitude noise in semiconductor lasers, which already has a long history, and of more recent interest, on the study of quantum noise in laser amplifiers and oscillators. Because squeezed light is intrinsically quantum mechanical, the study of its properties provides a unique opportunity to test predictions of quantum electrodynamics and observe new physics.

The important fundamental sources of intensity noise in a single-mode laser have been well known for some time. Intensity fluctuations at frequencies above the cavity bandwidth are due to the variance of the vacuum field that is reflected off the laser's front facet. Near threshold at frequencies below the cavity bandwidth, relaxation oscillations together with spontaneous emission are the primary sources of intensity noise. When such a laser is driven far above threshold, these noise sources are significantly reduced. Spontaneous emission is clamped at threshold. Relaxation oscillations are suppressed by gain saturation. At a sufficiently high pump rate, the remaining intensity noise will be due to fluctuations in the pump and vacuum field fluctuations entering through optical losses in the cavity.

Golubev and Sokolov first recognized that if an ideal laser that is driven far above threshold experiences sub-Poissonian fluctuations in the pump, then the laser output will also be sub-Poissonian, i.e. photon-number squeezed. Optical pump fields with sub-Poissonian fluctuations are clearly not readily available. Electrical current noise, however, does not have a shot-noise limit and is routinely reduced to levels limited by, for example, Johnson noise. Based on this concept, a group headed by Yamamoto developed the approach of high-impedance pump-noise suppression in semiconductors to achieve reduced noise in the intensity fluctuations leading to the first observation of photon-number squeezing (0.2 dB) from a semi-conductor device. A major extension of this development was made by our group on this program using quantum-well lasers at cryogenic temperatures which has enabled the demonstration of noise reduction to near the theoretical limit as well as the first demonstration of an application.

The pump statistics of a semiconductor laser are complicated by carrier dynamics in the active region. The high-impedance pump-noise suppression model predicts that if the laser is driven by a constant current source, then the fluctuations of the laser's pump will be due to noise on the electrical current. Hence, the laser's output field can be photon-number squeezed. This setup may be implemented for example by using a constant voltage source with an output series impedance much larger than the differential resistance of the lasing junction. In this arrangement, the theory

predicts that the pump noise is given by the source resistance Johnson noise, which is typically 20-30 dB below the corresponding optical shot-noise power. Given that the electrical drive current noise is negligible, squeezing inside the laser cavity is predicted to be limited to 50%; however, squeezing in the external field is predicted to be *only limited by the optical efficiency.* Experimental verification of this theory, demonstrating a connection between the laser photon-number squeezing and drive circuit source impedance, has not yet been made. However, a demonstration of the principle at noise levels above the SNL has been provided. A similar mechanism has been used to explain amplitude squeezing and quantum correlations observed in other light emitting semiconductor devices.

In this funding period we have focused on understanding the general disagreement between results from various optical configurations and the standard single-mode model for photon-number squeezing in semiconductor lasers along with achieving a demonstration of the application of this radiation. We have identified the suppression of longitudinal side modes, even in highly single-mode lasers, along with the use of polarization insenstive balanced dectors, as the primary requirements to obtain squeezing. In studies of the quantum noise properties of injection-locked laser oscillators, we found that suppression of the longitudinal side modes enhanced squeezing by more than 2 dB (recently to a maximum of 4.5 dB squeezing) at cryogenic temperatures. The use of dispersive feedback from a grating, in an external cavity configuration, results in 1.8 dB of photon-number squeezing at room temperature, tunable over a range in excess of 20 nm. Our recent demonstration that the drive current of an injection-locked semiconductor laser may be modulated without loss of squeezing opens the possibility for modulation applications of these photon-number squeezed lasers in communication and precision measurement. Finally, we have demonstrated improvement in the signal-to-noise beyond the standard quantum limit in a nonlinear laser spectroscopy measurement of the exciton and Urbach tail in a GaAs quantum well structure.

Quantum-well Laser Squeezing

In collaboration with Spectra Diode Laboratories, we have studied the amplitude noise characteristics of semiconductor quantum-well lasers under a wide range of optical configurations. The work has involved twelve lasers all of the SDL-5400 quantum-well family, several of which were taken from the same wafer. These lasers feature a highly single longitudinal and spatial mode output at room temperature, high quantum efficiency, and exceptional maximum I_{op}/I_{th} ratios (typically > 6), all of which make them excellent candidates for photon-number squeezing generation. Table 1 summarizes the squeezing results. The lasers were studied both at room temperature and cryogenic (10-77K) temperatures. Because the efficiencies of a given optical setup can vary, the squeezing at the laser front facet (corrected for optical losses in the setup) is provided in parentheses. As mentioned earlier, the single-mode high-impedance pump noise suppression model predicts that the limit to photon-number squeezing in the external field is the optical efficiency of the laser. This number is usually taken to be the laser's quantum efficiency. Several authors have suggested that because electrical losses within the semiconductor chip that are not involved in the lasing action may not introduce Poisson partition noise, the laser's apparent quantum efficiency may not be the ultimate limit. Although we have not observed squeezing beyond the quantum efficiency limit, Richardson, *et al.* have seen evidence in support of this picture. (NOTE: Similar data were obtained in our laboratory using a different laser but identical detectors following their report; however, in our case, we demonstrated the high level of apparent noise reduction was an artifact of high frequency saturation of the detector response.) Here we give the laser's total quantum efficiency ξ (at the drive current level of the measurement) as the theoretical limit to compare with our measured squeezing. If the lasers are driven sufficiently far above threshold, then the squeezing limit would become the laser's differential quantum efficiency, which is typically 0.78 (6.6 dB) at 10 K and 0.67 (4.8 dB) at room temperature.

The amplitude squeezing results show a wide variation between different optical configurations and an overall apparent disagreement with the theoretical predictions. The maximum squeezing

22

levels vary from 59% to 84% of the expected maximum from the quantum efficiency. This discrepancy is even greater when a comparison is made with the squeezing observed among all of the laser chips tested. Typically, when injection-locking or the external-cavity technique is used, the squeezing variation is approximately 0.5 dB. In the other free-running configurations, the squeezing varied from none to the maximum observed.

Temperature	Configuration	Experiment dB	η	Theory dB	% of Thry.
Cryogenic	Close-coupled	2.9 (3.7)	0.75	6.0	76
	Free-running	1.4 (2.4)	0.72	5.5	59
	Injection-locking	4.5 (5.9)	0.78	6.6	95
Room	Injection-locking	1.6 (2.1)	0.57	3.7	68
	External-cavity	1.8 (2.0)	0.51	3.1	72

TABLE 1. Summary of results of quantum-well semiconductor laser (SDL-5400) photon-number squeezing for various optical configurations; efficiency corrected squeezing at the laser output facet is given in parentheses; η=laser total quantum efficiency.

One aspect of our research has centered on understanding the fundamental quantum noise processes involved in the measurements of Table 1. In the next two sub-sections, we detail our work on the different configurations and examine the relevance of the single-mode high-impedance pump-noise suppression model to each configuration.

Injection-Locked Laser Oscillator

Injection-locked lasers have been studied extensively in the semi-classical regime. The van-der-Pole equation for a driven semi-classical oscillator describes the salient features in this limit. The output of an injection-locked laser is phase-coherent with the external driving field. Injection-locking has several well-known benefits that are expected to enhance squeezing. Dipole moment fluctuations are suppressed and the threshold current is reduced due to the enhanced stimulated emission at the locking frequency. Furthermore, longitudinal side mode amplitudes will be suppressed relative to the locked primary lasing mode.

The coherent locking of one or more squeezed lasers to an external field has important potential for applications. Interferometric measurements on the driving field may be enhanced by introducing the locked squeezed field to the open beam splitter port of the interferometer. Under certain limits, the photon-number squeezed field is predicted to be transformed into a (quadrature) squeezed vacuum field by interference with a coherent local oscillator field. Wiseman and Milburn have predicted that phase-locking a photon-number squeezed laser by external feedback can also result in quadrature squeezed output. The locked laser oscillator has many useful applications in communications for both detection and modulation. For example, frequency modulation of the external driving field results in stable phase modulation of the locked laser, with very low residual amplitude modulation.
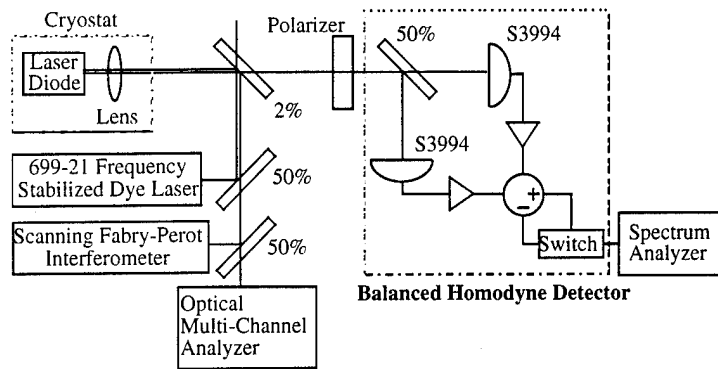
Figure 17. Optical setup for injection-locking a low temperature quantum-well semiconductor laser with a frequency stabilized, tunable dye laser.
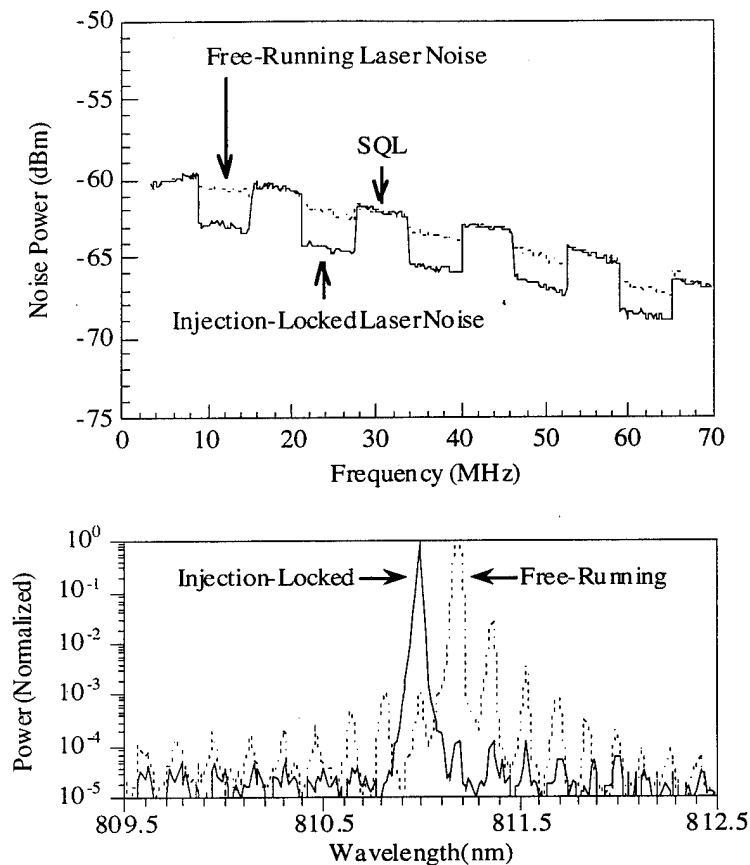

Figure 18. Amplitude noise spectra and longitudinal mode spectra of a semiconductor laser driven by the high-impedance pump noise suppression technique under both free-running and injection-locked conditions. The laser is held in a cryostat at 10K.

Our experiments on an injection-locked photon-number squeezed semiconductor laser driven by the high-impedance pump-noise suppression technique revealed a significant enhancement of the photon-number squeezing. This apparent discrepancy with predictions can be understood by considering noise due to weak longitudinal side modes, which are not accounted for in the theoretical treatments. The experiment setup for injection-locking a laser at low temperature is shown in Fig. 17. A frequency stabilized, tunable dye laser is used to injection-lock the laser diode. The laser noise and SNL are measured in a balanced homodyne detector, and the longitudinal mode spectrum is measured in an optical multi-channel analyzer. In Fig. 18, the amplitude noise spectra of the locked and unlocked laser are shown together with the corresponding longitudinal mode spectra. The amplitude noise is observed to drop from 1 dB below the SNL to more than 3 dB below upon injection-locking. In the longitudinal mode spectra, we see a correlated reduction by nearly two orders of magnitude of the side mode amplitudes.

24

Theoretical treatments of injection-locking have not considered the importance of multiple longitudinal modes on the amplitude noise spectrum. We have found that the suppression of the longitudinal side modes, even when they are already orders of magnitude below the primary lasing mode, leads to a significant enhancement in the magnitude of squeezing.

The suppression of longitudinal mode partition noise by optical injection techniques has enabled the observation by our group of more than 1.6 dB of photon-number squeezing at room temperature. Prior to this work, a maximum of 0.2 dB squeezing was observed at room temperature from a semiconductor laser. Correlations observed by our group between the longitudinal mode spectrum and the amplitude noise spectrum for lasers at low temperatures prompted attempts to suppress the side mode amplitudes. The success of this technique has enabled the reliable generation of photon-number squeezed light from room temperature lasers, which are viable sources for many practical applications. Longitudinal mode partition noise has long been recognized as an important noise source in semiconductor lasers. In the first observation by Yamamoto of photon-number squeezing from a semiconductor laser, mode partition noise was suggested as a possible limitation to the observed squeezing. Later measurements, however, revealed that due to quantum correlations between the amplitude fluctuations of various longitudinal modes, photon-number squeezing can be observed even in multi-mode lasers. This correlation is due to the homogeneously broadened semiconductor gain medium. Fast intraband carrier-carrier scattering allows for the very broad semiconductor longitudinal mode spectrum to couple to a single quasi-equilibrium upper state population. This coupling is expected to be enhanced at room temperature and hence cannot account for the lower squeezing numbers compared to low temperature results. Several non-linear gain and incomplete cross-mode gain saturation mechanisms have been suggested to account for the increased amplitude noise due to the presence of longitudinal side modes. Suppression of the side modes, which forces the laser behavior closer to that of an ideal single-mode laser, improves agreement with the single-mode high-impedance pump-noise suppression model.

External Cavity Quantum-well Laser

Semiconductor lasers are often used in external-cavity configurations because of the high stability and control that are provided by the extended macroscopic lasing cavity. A diffraction grating may be used in either a Littrow or a Littman (grazing incidence) configuration in order to provide dispersive feedback within the cavity (the combination of a birefringent filter and polarizer have also been used with similar results). The effect of such feedback can be to allow continuous or semi-continuous tuning over most of the semiconductor laser gain bandwidth with suppression of the longitudinal side modes. In recent experiments, we demonstrated that a tunable, single-source, room temperature photon-number squeezed laser may be constructed using a Littrow configured external-cavity. The maximum squeezing achieved from this laser at the output port was 1.8 dB.

For the observation of amplitude squeezing, the external cavity was used in a coupled cavity configuration with dispersive feedback rather than as an extended laser cavity. If a semiconductor laser is anti-reflection coated on one output facet such that it will not lase without external feedback, the laser may be thought of as a gain medium for the extended cavity (which includes the feedback element)--neglecting Fabry-Perot effects of the semiconductor chip. Semiconductor lasers used in this configuration were always found to exhibit noise at or above the SNL (typically 10 dB or more). The standard SDL-5400 series quantum-well laser has a 2-3% reflectivity output facet. This low output coupler reflectivity allows the laser to be used in external-cavity configurations even though it may operate far above threshold without feedback. In this coupled-cavity situation, the light returning from the dispersive element effects the laser in a manner similar to an external field injected from a separate source. The feedback serves to suppress longitudinal side modes and damp dipole moment fluctuations. The laser's threshold is also reduced, which allows for higher pumping. At present, an analytical theory does not exist to describe photon-

number squeezing in an external-cavity semiconductor laser. In the feedback regime that is used for squeezing, one might expect behavior similar to that observed in an injection-locking arrangement and this is consistent with our observations.

Squeezing results for an external cavity experiment are shown in Fig. 19. Photon-number squeezing is maintained to the maximum RF frequency observed in the detector response. The squeezing is also maintained upon tuning the external cavity wavelength over a 20 nm range. At short wavelengths, squeezing persists to the edge of the power tuning curve. On the long wavelength side, squeezing is lost five nanometers below the edge of the power tuning curve. Without dispersive feedback, the laser noise is 6 dB above the SNL. With feedback the noise drops to 1.8 dB below the SNL. The longitudinal side modes are suppressed due to the feedback by nearly three orders of magnitude to > 55 dB below the primary lasing mode.
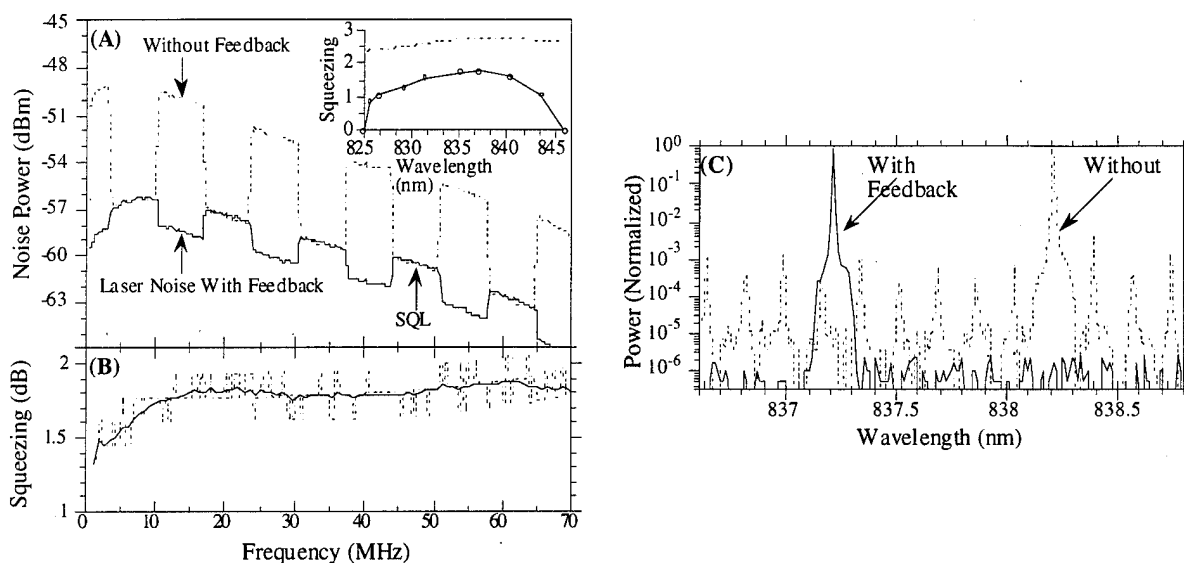

Figure 19. (A) Amplitude noise spectra obtained with (solid line) and without (dashed line) optical feedback from a Littrow configured grating. Both curves alternately display the laser noise and SQL. The inset shows the amplitude squeezing level obtained at a series of output wavelengths. The dashed line in the inset indicates the squeezing level possible based on total system efficiency. (B) The amplitude squeezing as a function of frequency corresponding to (A). (C) Monochromater scans taken concurrently with the amplitude noise spectra of (A).

A correction to the squeezing can be made for the efficiency (both diffraction and feedback coupling) of the diffraction grating for comparison with other laser configurations. When diffraction gratings with different efficiencies were used in the external cavity, the amplitude squeezing was degraded, as expected for a lossy optical element. In fact, Littman configuration external-cavity lasers were found to produce poor squeezing due to the low efficiency of the double first-order diffraction feedback. This observation identifies the grating losses as an important design parameter of photon-number squeezed sources with dispersive feedback.

Polarization Dependent Noise

Noise from competing polarization fields in a semiconductor laser is found to have large fluctuations that can influence both the laser's amplitude noise and the SNL calibration measurement in a balanced detector. Because of very high extinction ratios in semiconductor lasers (often >400:1), the weak polarization perpendicular to the lasing junction is frequently neglected. At low temperatures and near threshold, however, the extinction ratio can be less than 100:1. Because of the dipole moment selection rules, each polarization couples to a different population in the gain medium. Like the longitudinal modes, carrier scattering (if an electron spin flip occurs)

26

will result in gain saturation across the two polarizations. Thus, amplitude fluctuations on the weak polarization may be correlated with fluctuations on the primary polarization field.

In certain balanced homodyne detector configurations, either quadrature or amplitude fluctuations of the weak polarization can appear on the difference current, destroying the SNL measurement. In a detector arrangement that uses a polarizing beam splitter with a 45° half-wave plate, the weak polarization enters the open port of the beam splitter. In this situation, the difference current is measuring quadrature fluctuations (depending on the phase relationship between the two polarizations) of the weak polarization, *not* the SNL for the primary polarization field. Therefore, a polarizer must be used with the balanced homodyne detector in this setup to remove the weak polarization. When a 50/50 plate beam splitter is used, fluctuations from the weak polarization can again show up on the difference current if the splitting ratio is not equal for both polarizations. Again, a polarizer can alleviate this problem or a non-polarizing plate beam splitter may be used.
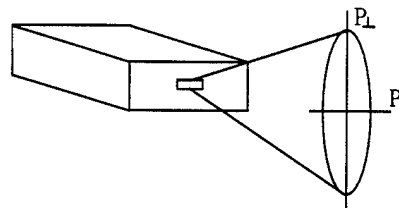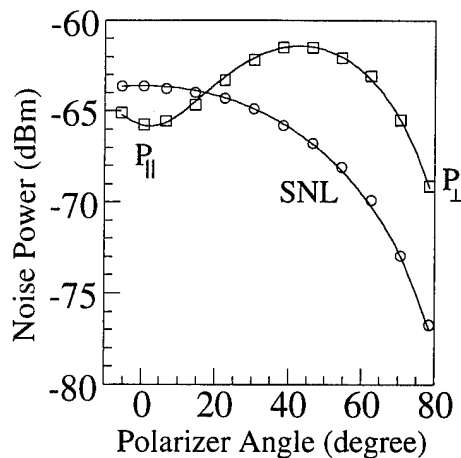

Figure 20. Polarization dependent noise. (left) Amplitude fluctuations as a function of polarization angle are measured for an injection locked laser at 10K. (above) Semiconductor emission polarization. Extinction ratio $P_{\parallel}$:$P_{\perp}$ is near 100:1.

Figure 20 shows measurements that were made of the polarization dependence of the amplitude noise. The measurements were taken by rotating a half-wave plate in front of a polarizer that was placed at the entrance to a balanced homodyne detector. This setup ensured correct measurement of the SNL on the difference current. Fluctuations on the weak polarization were found to be 8 dB above the corresponding SNL; whereas, the fluctuations on the primary polarization are observed to be 2.2 dB squeezed. The data was taken using the output of an injection locked laser at cryogenic temperatures. A simple model for mixing the photon-number fluctuations of two single mode fields is found to be an excellent fit to the data.

Further studies, however, demonstrated that while the use of a polarizer in front of the polarization dependent beam splitter in the balanced detector improved the degree of measurable squeezing, in fact the overall polarization dependence of this approach suppressed important correlations in the optical beam which in fact limited the amount of detectable noise reduction. Specifically, we demonstrate that noise measurements of the photon-number squeezed light from a quantum-well laser are indeed influenced by the polarization properties of the laser output itself. Observations of the total (polarization preserved) output of an injection-locked low temperature laser reveal photon-number squeezing that is more than 1 dB improved over measurements of the linearly polarized laser output and within 95% of the predicted maximum squeezing based on the device quantum efficiency. Polarization sensitivity in the data is accounted for by amplitude noise processes that include the effects of birefringence and quantum correlations generated in the laser.

The optical configuration used in this experiment is shown in Figure 21, and differs from the earlier set up as it was designed to virtually eliminate the polarization dependence.
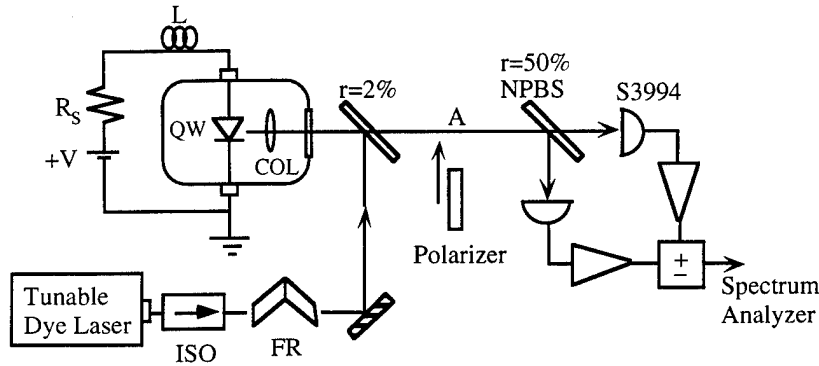

Figure 21. Experiment setup. QW: quantum well laser; ISO: isolator; FR: Fresnel Rhomb; COL: collimating lens; NPBS: non-polarizing beamsplitter.

The polarization dependent amplitude noise spectra from the laser are shown in Figure 22a. Trace A shows the power spectrum of the laser output without polarization analysis. The noise level is 3.0 dB below the SNL over most of the frequency range shown. The SNL is measured on the difference current of the balanced homodyne detector (27 dB gain) and confirmed with a red-filtered Halogen lamp noise spectrum. The polarization sensitivity of the laser noise is seen in traces B and C (relative average optical power between the two traces is 170:1, respectively). When a linear polarizer (ext. ratio 10^4:1) is introduced at point A (see Figure 21) and aligned for maximum transmission, which corresponds to the polarization axis parallel to the laser junction, the squeezing is reduced (i.e. noise increased) by approximately 2 dB. This increase in noise cannot be accounted for by the optical loss (2%) due to the polarizer. The SNL trace shown is, in fact, the difference current spectrum of the polarized field and agrees with the SNL for the unanalyzed field to within the spectrum analyzer resolution (0.1 dB), as expected. Trace C shows the spectrum that results when the polarizer is aligned for minimum transmission, which corresponds to the polarization axis perpendicular to the laser junction.
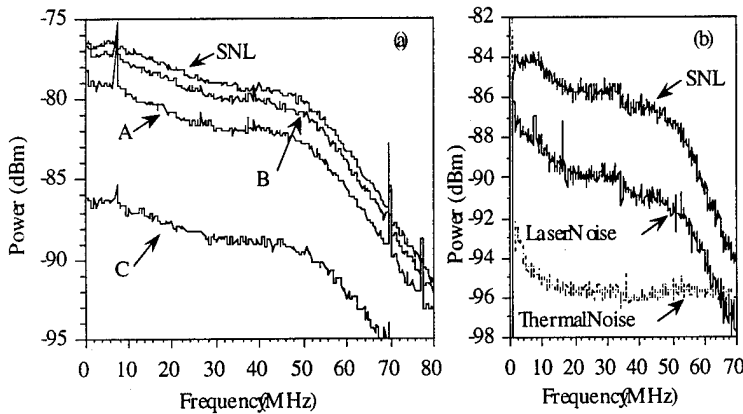

Fig. 22. (a) Photocurrent power spectra for linearly polarized output parallel (trace B) and perpendicular (trace C) to the laser junction, and the unanalyzed (trace A) laser output. SNL is the measured shot noise level for both the parallel polarized and unanalyzed fields; spectrum analyzer: 300 kHz RBW, 3 kHz VF, 10 scan avg. (b) Photocurrent power spectrum for laser optimized to achieve maximum squeezing (4.5 dB). Laser Noise trace is the unanalyzed laser noise; s. a.: 100 kHz RBW, 10 kHz VF, no avg. The electronic thermal noise has been subtracted from each trace.

The noise increase when a polarizer is introduced can be accounted for by the presence of photon-number fluctuations that are anti-correlated between orthogonally polarized fields at the detector. When the unanalyzed laser output is incident on the photodetector, the anti-correlated photon-number fluctuations cancel and the low noise trace A in Figure 22a is observed. However,

if the fluctuations on one polarization are blocked by introducing a polarizer, then this cancellation cannot occur and the noise increases. Thus, the use of polarization-preserving detection optics is necessary to suppress such polarization dependent noise. We note that great care has been taken to ensure that these results are not due to effects such as spurious feedback or detector saturation

The largest photon-number squeezing obtained in this configuration is shown in Figure 22b. The Laser Noise trace is the power spectrum of the laser output without polarization analysis. The noise level is 4.5 dB below the SNL in the range 20-45 MHz. The SNL is measured with a balanced homodyne detector (20 dB gain) and confirmed as above. Correcting for the losses in the optical setup (13%), the squeezing at the laser front facet is 5.9 dB. If the internal optical loss is accounted for by the laser quantum efficiency at 15K (78%), then this value is within 95% of the expected maximum squeezing. For the two lasers that were tested, the squeezing was observed to closely approach, but never exceed this limit for drive currents up to 75 times threshold.

In order to determine the origins of the polarization dependent noise shown in Figure 22a calculations of the amplitude noise spectra that result from two orthogonally polarized fields in the laser output have been carried out for various polarization conditions. The photon-number variances are determined for each case using: $\langle \Delta n^2 \rangle = \langle (n - \langle n \rangle)^2 \rangle$. The photon-number variance of the total output field of a semiconductor laser in the absence of birefringence is given by: $\langle \Delta n_o^2 \rangle = \langle \Delta n_{\parallel}^2 \rangle + \langle \Delta n_{\perp}^2 \rangle + \langle \Delta n_{\parallel} \Delta n_{\perp} + \Delta n_{\perp} \Delta n_{\parallel} \rangle$. The first two terms are the photon-number variances corresponding to the parallel and perpendicularly polarized laser output fields, respectively. The third term will be non-zero if the output fields have correlated photon-number fluctuations. If the covariance term is negative, then the noise on the parallel polarized field $\langle \Delta n_{\parallel}^2 \rangle$ may be larger than the noise on the unanalyzed field $\langle \Delta n_o^2 \rangle$. The results in Figure 22a may be entirely accounted for by such intrinsic correlations with a degree of correlation $(1/2)\langle \Delta n_{\parallel} \Delta n_{\perp} + \Delta n_{\perp} \Delta n_{\parallel} \rangle / \sqrt{\langle \Delta n_{\parallel}^2 \rangle \langle \Delta n_{\perp}^2 \rangle}$ equal to -0.70 in the range 5-40 MHz, decreasing to -0.55 at 80 MHz. In this situation, the weak perpendicularly polarized field has noise far above the corresponding SNL (which is >20 dB below the SNL in Figure 22a), but nevertheless holds quantum information about the photon number in the squeezed parallel polarized field.

Such fundamental correlations are potentially significant, but we note that birefringence in the optics or laser could also lead to similar behavior. Using a rigorous quantum optical description, the effects of birefringence on the laser output have been evaluated. After passing through a birefringent element, the two orthogonally polarized components can become elliptically polarized, but remain orthogonal and will not mix on a photodetector. When a polarizer is introduced, however, the projections of the orthogonal field components onto the polarizer axis will interfere. The homodyne beating that arises because the fields are mixed in the presence of birefringence is equal in magnitude and anti-correlated between the two orthogonal polarization analysis directions. Such anti-correlated fluctuations, which are expected from energy conservation, will be present even if the orthogonally polarized laser output fields are uncorrelated.

Although birefringence alone can generate behavior that is qualitatively similar to correlated photon-number fluctuations in the laser, in fact the analytical results, which only take into account birefringence external to the laser cavity, show that birefringence cannot account for the data in Figure 22a. Because such noise due to birefringence makes an equal contribution to each polarized noise spectrum, given the relative magnitude of fluctuations measured along each polarization axis, the largest correlation that could result from birefringence alone is -0.41, which is clearly less correlated than the observed -0.7. Nevertheless, one cannot rule out a contribution from noise due to birefringence, particularly if significant birefringence exists inside the laser cavity.

Evidence of quantum correlated polarization dependent fluctuations can be expected due to nonlinear polarization coupling in the semiconductor laser gain medium. If the rate of carrier spin relaxation is much faster than the stimulated recombination rate, then gain saturation across the polarization modes can occur. In this event, emission along the two polarization axes will couple to the same upper state population and experience quantum correlated amplitude fluctuations in much the same manner that quantum correlations arise between different longitudinal modes.

Modulation Studies

An important step in the application of squeezed light generated by quantum-well semiconductor lasers is the modulation of the optical field with sensitivity below the SNL. Modulation is an essential part of many types of ultra-sensitive optical spectroscopy and communication technologies. In many applications it is necessary that the fidelity of the optical signal is maintained at both the signal frequency and outside the signal frequency. Frequency division multiplexing, for example, requires that modulation at one frequency does not introduce noise at other frequencies.

The modulation of the drive current of a semiconductor laser is a common technique that is simple to realize in practice, but often accompanied by an increase in noise. In the high-impedance pump-noise suppression model, the statistics of the regular pump current can be the limiting noise source on the output photon flux. In this linearized, single-mode model, the introduction of a time varying component to the pump current should modulate the output field without introducing noise. Because the amplitude and phase of the optical field are both influenced by the drive current through the linewidth enhancement factor, frequency (or phase) and amplitude modulation will both result from drive current modulation. Other non-linear effects common in semiconductor lasers can introduce modulation dependent noise. Modulation through external techniques (AOMs, choppers) introduce noise due to the necessary optical losses incurred. Current modulation of semiconductor lasers has the potential to achieve a modulated optical field without the introducing additional quantum noise.
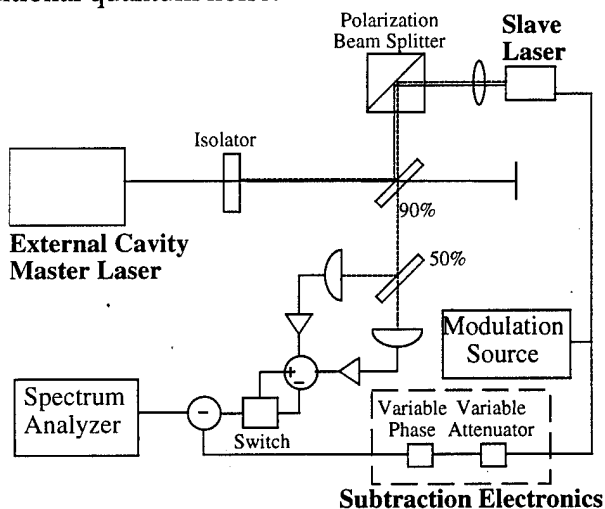

Figure 23. Experiment setup for measurement of modulation noise both at the modulation frequency and over the entire amplitude noise spectrum. The detectors are attached to liquid N_2 cold fingers in order to increase the frequency response, which is transit time limited.

Squeezing measurements were made of the photocurrent power spectrum at all frequencies of interest, in particular, at the modulation frequency. Figure 23 shows the setup for measuring the laser noise properties under direct drive current modulation. The subtraction electronics, noted in the figure, are used to remove the large classical modulation signal from the detected rf spectrum, so that the noise at the modulation frequency may be observed. Cancellation of a modulation signal by subtraction of an amplitude and phase matched reference is limited by the noise on the modulation signal. Thus, the best cancellation that may be achieved is a measure of the noise at the

modulation frequency. When measuring the noise outside the modulation frequency, the subtraction electronics are removed.

The drive current may be modulated at all frequencies tested (50-400 MHz) without loss of squeezing over the entire spectrum (including at the modulation frequency), up to the maximum power levels permitted by the drive current and detection electronics. Figure 24 shows the typical results of a modulation experiment. The power spectrum is shown both with the modulation signal (trace c) and when the modulation signal has been removed (trace b). The inset clearly shows that, within the spectrum analyzer resolution bandwidth, squeezing is maintained at the modulation frequency. In separate measurements using a broadband source, the laser noise was further confirmed to be 0.8 dB squeezed within the source bandwidth. The laser noise spectrum is squeezed by approximately 0.8 dB over the entire spectrum. Squeezing values closer to the observed maximum (1.6 dB) would be possible with the use of a different laser chip and higher quantum efficiency optics and detectors.
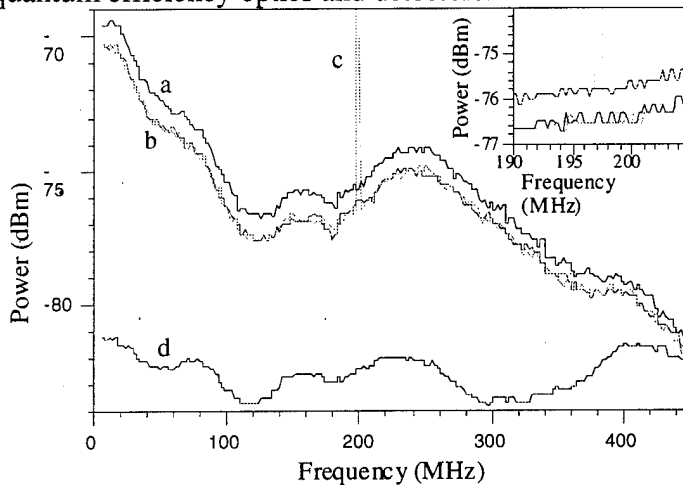

Figure 24. Amplitude noise spectrum of a drive current modulated, injection-locked laser: Trace (a) is the SNL. Trace (b) is the laser noise with the modulation signal subtracted from the photocurrent. Trace (c) is the unmodified photocurrent. 0.8 dB amplitude squeezing is observed over the full spectrum, not degraded by the large modulation signal; Inset shows expanded view near the modulation frequency. Trace (d) is the detector noise floor.

These modulation experiments demonstrate that signals may be generated by a quantum-well semiconductor laser with signal to noise ratios that, given equal modulation powers, may only be achieved with a nonclassical source. Furthermore, nonclassical, quiet operation may be maintained over the entire spectrum of squeezing in the presence of modulation.

Measurement of the Semi-Classical Shot-noise Limit

An important aspect of any squeezing work is the proper determination of the semi-classical shot-noise limit. Although photon-number squeezing has the advantage that its benefits are realized by direct detection with a single photodetector, in order to make accurate measurements of the level of fluctuations below the SNL the use of a balanced homodyne detector is very important. Single detector measurements of the SNL by comparison with classical light sources (e.g. gas lasers, low efficiency LEDs, filtered Halogen lamp sources) are sensitive to detector saturation effects that may depend on beam spot size, spectral distribution, intensity profile, etc. The requirement that the semiconductor laser be driven far above threshold introduces power levels on the order of 10-100 mW, above the saturation power of many photodetectors. Furthermore, in some cases when the DC detector response may show very little saturation, the high frequency response is highly non-linear. The balanced homodyne detector, however, allows for the simultaneous measurement of the laser noise and SNL under *identical experimental conditions*. Since the same photocurrent is used to make both measurements, saturation effects will to first order influence both measurements equally. Thus, balanced homodyne detection is largely insensitive to detector saturation.

Of particular concern, even in balanced homodyne detector measurements, are highly non-linear, breakdown type saturation effects. For use in the close coupled experiments and to verify that our measurements are not influenced by large non-linearities in the detectors, we have made careful measurements of the frequency response characteristics of several photodetectors, including the two types used in our measurements. In the measurement of amplitude noise spectra (typically 1-1000 MHz), we have observed several different types of detector saturation mechanisms, each of which depends on the type of detector response: either RC-time-constant-limited or transit-time-limited. The Hamamatsu S3994 detectors used in much of our work were found to have highly linear characteristics with a very gradual saturation of the frequency response. This is expected from a detector with a frequency response that is primarily RC-time-constant-limited. Detectors that are limited by transit time effects, however, can have dramatic saturation behavior, usually associated with thermal effects. The Hamamatsu S1722-01 detector, which is transit time limited, was found to have a gradual saturation response similar to the S3994. However, when the laser spot overfills the detector, illuminating the silicon wafer substrate, the high frequency response is lower than expected for the measured DC level. This is most likely due to a long transit time in the silicon wafer region. The spot size on the detector was found to significantly influence the detector saturation properties in transit time limited detectors when the diameter is less than 1.0 mm. The NEC NDL-2208 detector, which is also limited by the electron transit time and has an active area only 0.1 mm across, shows a gradual saturation at low power levels and an abrupt collapse in the response that may occur at as small as a 9.7 mA (cryogenicly cooled) detector current (equal to or less than the level used in many squeezing experiments).

Careful calibration of the SNL together with verification of the non-classical attenuation property of squeezed light is an important part of this work. In all of our measurements, except for the close-coupled laser experiments (for obvious reasons), balanced detector measurements were used. In addition, the SNL was confirmed by comparison with a red-filtered halogen lamp and/or a high-power LED array. Furthermore, the presence of squeezing was confirmed by attenuation of the beam with one or more neutral density filters. An increase in noise upon attenuation, due to introduction of the vacuum field fluctuations, is a strong confirmation of squeezing.

Application of Amplitude Squeezed Light:

In the first demonstration of amplitude squeezed light, we used photon-number squeezed light generated by an injection-locked quantum-well laser as the probe field in a coherent non-linear optical (pump-probe) spectroscopy measurement of the Urbach tail and exciton resonances in a GaAs multiple quantum-well sample. The resulting spectrum is shown in Figure 25. The measured photon-number squeezing in the probe field without the sample present is shown in the inset of Figure 25. The arrow indicates the signal frequency, at which 1.9 dB of squeezing, which is approximately the squeezing of the field incident on the sample, is observed. The semiclassical shot noise limit (SNL) is determined by the difference photocurrent of the balanced homodyne detector. Due to the 1.9 dB squeezed intensity fluctuations of the probe field incident on the sample, the measurement sensitivity in this experiment is 1.0 dB (20%) below the SNL. This sensitivity enhancement is evident at the low frequency end of the Urbach tail where the signal amplitude falls below the SNL. The measured quantum noise level is nearly one-third (below the SNL) of the fundamental nonclassical sensitivity limit (5.2 dB below the SNL) set by the vacuum field fluctuations that enter through background losses (30%) in the sample. The 1.9 dB squeezing level is reduced to 1.0 dB when the sample is present, due to such vacuum field fluctuations introduced through sample losses and polarization dependent noise coupled into the amplitude noise spectrum through the polarization dependence of the sample transmission.
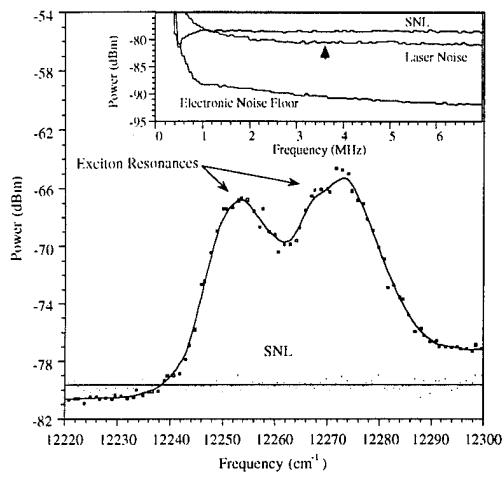
Figure 25. GaAs multiple quantum-well coherent nonlinear optical spectrum. The measurement sensitivity, evident in the low frequency Urbach tail, is 1.0 dB below the semiclassical shot noise limit (SNL), after 30% attenuation in the sample. Inset: amplitude noise spectrum with the sample removed. The arrow indicates the signal frequency and 1.9 dB of squeezing.

II.B. PUBLICATION SUMMARY

II.B.1 PUBLICATIONS IN REFEREED JOURNALS

M. Freeman, H. Wang, D.G. Steel, D. Scifers, R. Craig, "Amplitude Squeezed Light from Quantum-well Lasers," Opt. Lett. **18**, 379-381 (1993).

Hailin Wang, Kyle Ferrio, Duncan G. Steel, Y. Hu, Rolf Binder, Stephan Koch "Transient Nonlinear Optical Response from Excitation Induced Dephasing in GaAs," Phys. Rev. Lett. **71**, 1261-1264 (1993).

Min Jiang, Hailin Wang, R. Merlin, M. Cardona D.G. Steel, "Nonlinear optical spectroscopy in GaAs: Magnetic freezeout of excitons," Physical Review B, Rapid Communiciations, **48**, 15476-15479 (1993).

Hailin Wang, Michael J. Freeman, Duncan G. Steel, "Squeezed light from injection locked quantum-well lasers," Phys. Rev. Lett. **71**, 3951-3954 (1993).

M. J. Freeman, H. Wang, D.G. Steel, R. Craig, D. R. Scifres, "Wavelength-tunable amplitude squeezed light from a room temperature quantum-well laser," Opt. Lett. **18**, 2141-2143 (1993).

H. Wang, K.B. Ferrio, D. G. Steel, P. R. Berman, Y. Z. Hu, R. Binder, S.W. Koch, "Transient four-wave mixing line shapes: effects of excitation induced dephasing," Phys. Rev. A, **49**, 1551-1554 (1994).

Y.Z. Hu, R. Binder, S. W. Koch, S. T. Cundiff, H. Wang, D.G. Steel, "Excitation and polarization effects in semiconductor four-wave-mixing spectroscopy," Phys. Rev. B **49**, 14382-14386 (1994).

Mike Freeman, Dan Kilper, Duncan Steel, "Room-temperature amplitude-squeezed light from an injection-locked quantum-well laser with a time-varying drive current," Opt. Lett. **20**, 183-185 (1994).

Min Jiang, A. C. Schaefer, D. G. Steel, "Polarization Dependence of the Frequency Domain Four-Wave Mixing Response of Excitons in GaAs", Phys. Rev. B, **51**, 16714-16720 (1995).

K. B. Ferrio and D.G. Steel "Excitation-Induced Optical Nonlinearities in GaAs" Laser Physics, **5**, 621-627 (1995).

K. B. Ferrio and D. G. Steel, "Observation of the Ultrafast Two-Photon Coherent Oscillation in a GaAs/AlGaAs Multiple-Quantum-Well: a Signature of Biexcitonic Optical Nonlinearity", submitted.

D. C. Kilper and D. G. Steel, "Polarization dependent noise in photon-number squeezed light generated by quantum-well lasers," accepted, Optics Letters (1996).

D. C. Kilper, A. C. Schaefer, J. Erland[a] and D. G. Steel, "Coherent nonlinear optical spectroscopy using photon-number squeezed light," submitted (1996).

K.B. Ferrio and D.G. Steel, "Detection of the Raman induced Heavy-Hole-Light-Hole Quantum Coherence," in preparation

N. Bonadeo, R. Merlin, D.G. Steel, "Polarization Transfer in the Excitonic Free Polarization Decay," in preparation.

N. Bonadeo and D.G. Steel, "Polariton Beats," in preparation

A. Schaefer and D.G. Steel," Failure of Fick's Law in Excitonic Transport: Ballistic Exciton Motion," in preparation.

II.B.2. BOOK CONTRIBUTIONS
Duncan G. Steel, Hailin Wang, Min Jiang, Kyle Ferrio, Steve Cundiff, "Nonlinear Coherent Optical Effects in Semiconductors, " *invited paper* to be published in the Proceedings of the NATO ARW on Coherent Optical Interactions in Semiconductors, Cambridge, 1993.
A.C. Schaefer and D.G. Steel, " Resonant Nonlinear Optical Behavior in Undoped GaAs Quantum-wells," in *Properties of III-V Quantum-wells and Superlattices,* P.K. Bhattacharya, ed. (1995)

II.B.3. INVITED PAPERS
Duncan G. Steel, Hailin Wang, Steve Cundiff, Min Jiang, Kyle Ferrio, Anne Schaefer, "Coherences and Dynamics of Resonances in Semiconductor Heterostructures," Workshop on Optical Properties of Mesoscopic Semiconductor Structures, Snowbird, 1993.

H. Wang, Kyle Ferrio, D.G. Steel, "Excitation Induced Dephasing," ILS'94.

D.G. Steel, Kyle Ferrio, H. Wang, Min Jiang, Anne Schaefer, "The role of exciton interactions in the GaAs nonlinear optical response," International Workshop on Lasers, 1994

Duncan G. Steel, Min Jiang, Anne Schaefer, Nicholas Bonadeo, Kyle Ferrio, "Four-wave mixing experiments on semiconductors," Radiative Processes and Dephasing in Semiconductors, 1994.

D.G. Steel, "Coherent optical interactions in semiconductor heterostructures," invited lecturer, Phillips Universität, Marburg (1994).

D.C. Kilper, M.J. Freeman, J. Erland, D.G. Steel, R. Craig and D.R. Scifres, "Amplitude Squeezed Light Generated by Semiconductor Quantum-well Lasers," QELS'95, OSA Technical Digest **16**, p16 (1995).

D.C. Kilper, M.J. Freeman,, D.G. Steel, R. Craig and D.R. Scifres, "Non-classical Amplitude Squeezed Light Generated by Semiconductor Quantum-well Lasers," Los Angeles, SPIE'95.

D.G. Steel, "Role of Disorder in Quantum Coherence, " invited Lecturer, Marburg Workshop on Disorder (1995)

D.G. Steel "Effects of Optical Induced Coherences in Semiconductors: An Overview", ILS'95.

II.B.4. CONFERENCES AND PROCEEDINGS

Kyle Ferrio, Hailin Wang, D.G. Steel, Y.Z. Hu, R. Binder, S.W. Koch, "Strong contribution of excitation-induced dephasing to the nonlinear-optical response of heavy-hole excitons in GaAs," ILS'93 Opt. Soc. Am. '93 (Toronto), 1993.

H. Wang, M. J. Freeman, D. G. Steel, R. Craig and D.R. Scifres, "Amplitude-Squeezed Light by Injection-Locking of Quantum-well Lasers ", Conference on Quantum Electronics and Laser Science (QELS'93)

Hailin Wang, Kyle Ferrio, and Duncan Steel, "Polarization dependent transient nonlinear optical response of heavy and light hole excitons in GaAs," Conference on Quantum Electronics and Laser Science (QELS'93).

M. Freeman, Hailin Wang, Duncan G. Steel, D. Scifers, H. Craig, "Amplitude Squeezing in a Semiconductor Quantum-well Laser," Conference on Quantum Electronics and Laser Science (QELS'93).

Min Jiang, Hailin Wang, Roberto Merlin, D.G. Steel, "Nonlinear optical response of magneto-excitons in GaAs," Conference on Quantum Electronics and Laser Science (QELS'93).

M. Freeman, Hailin Wang, Duncan G. Steel, D. Scifers, H. Craig, "Amplitude-Squeezed Light by Injection-Locking of Quantum-well Lasers" Conference on Quantum Electronics and Laser Science (QELS'93), QPD1.

Anne C. Schaefer, Min Jiang, Duncan G. Steel, "Investigation of the Optically Induced Increase of the Effective Excitonic Oscillator Strength in GaAs Distinct Higher-Order Nonlinear Optical Response for Spin-Dependent and Spin-Independent Contributions to Four Wave Mixing," IQEC'94.

K. B. Ferrio, Hailin Wang, Vinod Subramaniam, and Duncan G. Steel "Distinct Higher-Order Nonlinear Optical Response for Spin-Dependent and Spin-Independent Contributions to Four Wave Mixing", IQEC'94

A. Schaefer, M. Jiang, D. Steel, "Nonlinear Induced Absorption in GaAs: Evidence of Excitation Induced Decay" , APS Meeting, March, 1994.

Min Jiang, A. C. Schaefer, D.G. Steel "Measurement of the Red Shift due to Spin-Dependent Nonlinear Interactions in GaAs", IQEC'94

M. J. Freeman, H. Wang, and D. G. Steel, R. Craig and D. R. Scifres, "Room Temperature Wavelength-Tunable Amplitude Squeezed Light from a Quantum-well Laser", IQEC 94.

N. H. Bonadeo, M. Jiang, Vinod Subramaniam and D. G. Steel "Polarization studies of the free polarization decay on GaAs: Evidence for Excitonic Coherence Transfer", QELS'95, OSA Technical Digest **16**, p259-260 (1995).

D. C. Kilper, J. Erland, and D. G. Steel, "Ultra-sensitive Measurement with Amplitude Squeezed Light" QELS'95, OSA Technical Digest **16**, p72-73 (1995).

A. C. Schaefer, N. H. Bonadeo and D. G. Steel, "Transition to a Multiphoton Excitonic Response in GaAs" QELS'95, OSA Technical Digest **16**, p256 (1995).

A. C. Schaefer, J. Erland, D.G. Steel, "Non-Diffusive Excitonic Transport in GaAs: Evidence for Polariton Propagation, "QELS'95, OSA Technical Digest **16**, p114-115 (1995).

K. B. Ferrio, Nicolas Bonadeo, and Duncan G. Steel, Makoto Kuwata-Gonokami, "1.3-Femtosecond Oscillation of the Quantum Coherence in a GaAs Multiple-Quantum-Well: Observation of the Two-Photon Coherently Excited Biexciton," QELS'95, OSA Technical Digest **16**, p246 (1995).

N. H. Bonadeo, R Merlin and D. G. Steel, "Ultrafast Electric Field Polarization Evolution in the Excitonic Free Polarization decay of GaAs," QELS'96, accepted.

K. B. Ferrio, J.R. Guest, and Duncan G. Steel, "Anomalous decay and polarizatio nof electronic Raman coherence in GaAs," QELS'96, accepted.

A. C. Schaefer and D. G. Steel, "The effects of momentum scattering on exciton motion: Observation of non-diffusive transport," QELS'96, accepted.

D. C. Kilper, A. C. Schaefer, J. Erland[a], and D. G. Steel, "Coherent nonlinear optical spectroscopy using photon-number squeezed light" QELS'96, accepted.

II.C.   EDUCATIONAL TRAINING SUMMARY

The educational opportunity provided by this program has been outstanding as measured by the number and quality of students working on and completing their doctoral studies. In addition, this program has provided an educational opportunity for undergraduate students interested in obtaining research experience in physics and engineering.

During this research period, two students have graduated with their Ph.D. and three other students will complete their doctoral work within the next nine months. One former student supported by this program has just joined the faculty at a major university and a second student is now at AT&T Bell labs.